Power management optimization of hybrid power systems in electric ferries

Al-Falahi, Monaaf D.A.; Nimma, Kutaiba S.; Jayasinghe, Shantha D.G.; Enshaei, Hossein; Guerrero, Josep M.

Published in:
Energy Conversion and Management

DOI (link to publication from Publisher):
10.1016/j.enconman.2018.07.012

Publication date:
2018

Document Version
Early version, also known as pre-print

Power Management Optimization of Hybrid Power Systems in Electric Ferries

Monaaf D.A. Al-Falahi[a,*], Kutaiba S. Nimma[a], Shantha D. G. Jayasinghe[a], Hossein Enshaei[a],and Josep M. Guerrero[b]
[a] Australian Maritime College, University of Tasmania, Newnham, TAS 7248, Australia
[b] Institute of Energy Technology, Aalborg University, Aalborg 9220, Denmark
e-mail: *monaaf.alfalahi@utas.edu.au; kutaiba.sabah@utas.edu.au; shanthaj@utas.edu.au; hossein.enshaei@utas.edu.au, joz@et.aau.dk

***Abstract*—**The integration of more-electric technologies, such as energy storage systems (ESSs) and electric propulsion, has gained attention in recent years as a promising approach to reduce fuel consumption and emissions in the maritime industry. In this context, hybrid power systems (HPSs) with direct current (DC) distribution are currently gaining a commendable interest in research and industrial applications. This paper examines the impact of using HPS with DC distribution and a battery energy storage system (BESS) over a conventional AC power system for short haul roll-on/roll-off (RORO) ferries. An electric ferry with a HPS is modeled in this study and the power management system is simulated using the Matlab/Simulink software. The result is validated using measured load profile of a ferry. The performance of the DC HPS is compared with the conventional AC system based on fuel consumption and emission reductions. An approach to estimate the fuel consumption of the diesel engine through calculation of specific fuel oil consumption (SFOC) is also presented. This study uses two optimization techniques: a classical power management method namely Rule-Based control (RB) and a meta-heuristic power management method known as Grey Wolf Optimization (GWO) to optimally manage the power sharing of the proposed HPS. Fuel consumption and emission indicators are also used to assess the performance of the two power management methods. The simulation results show that the HPS provides a 2.91 % and 7.48 % fuel consumption reduction using RB method and GWO method respectively. It is apparent from the result that the HPS has more fuel savings while running the diesel generator sets (DGs) at higher operational efficiency. It is interesting that the proposed HPS using both power management methods provided a 100 % emission reduction at berth. Finally, it was found that using a meta-heuristic optimization algorithm provides better fuel and emission reductions than a classical method.

Keywords— Battery, DC power system, electric ferry, energy storage system, hybrid power system, power management.

Nomenclature

E_B	BESS energy [kWh]	g	DG operating variable [0 or 1]
FC_{berth}	Fuel consumption at berth [L]	η	Efficiency
$FC_{cruising}$	Fuel consumption while cruising [L]	θe	Electrical angle
FC_m	Fuel consumption at a certain operating condition [L]	θr	Rotor angle
N_S	Number of stops per ferry round-trip	λ	Ratio of load
N_p	Number of poles	*Abbreviation*	
P_B	BESS power [kW]	BESS	Battery energy storage system
P_{EL}	Instantaneous power at the specified engine load [kW]	CO_2	Carbon dioxide
P_L	Load power [kW]	DG	Diesel generator-set
P_{cha}	Charging power [kW]	ESS	Energy storage system
P_{dcha}	Discharging power [kW]	GWO	Grey wolf optimization
P_n	Generated power from n-th DG [kW]	HPS	Hybrid power system
P_n^{max}	Maximum power of n-th DG [kW]	IMO	International marine organization
P_{rated}	Rated power of DG (maximum power) [kW]	NO_X	Nitrogen oxide
P_{tn}	Power generated by n-th DG at t-th time [kW]	PMS	Power management strategy
$SFOC_{EL}$	SFOC value at specified engine load [L/kWh]	RB	Rule-based
$SFOC_n$	SFOC of n-th DG	RES	Renewable energy source
SOC^{high}	Upper SOC limit [%]	RORO	Roll-on/roll-off
$SOC^{initial}$	Initial SOC [%]	SO_X	Sulfur oxides
SOC^{max}	Maximum SOC [%]	*Subscripts*	
SOC^{min}	Minimum state of charge [%]	t_c	The index time of charging

e_{berth}	Emissions at terminal (berth) [g/kWh]	*B*	Battery
$e_{cruising}$	Emissions while cruising [g/kWh]	*bus*	Bus
Δt	Time step	*cha*	Charging
DoD	Depth of discharge [%]	*discha*	Discharging
E	Energy [kWh]	*EL*	Engine load
e	Emission [g/kWh]	*L*	Load
EL	Engine load	*loss*	Power loss
FC	Fuel consumption [L]	*m*	Operating condition
FC_{total}	Total fuel consumption of one round trip [L]	*max*	Maximum
i	Current (A)	*min*	Minimum
N	Number of DGs	*n*	n-th DG
R	Resistance [Ω]	*prop*	Propulsion
SFOC	Specific fuel oil consumption [L/kWh]	*ref*	Reference
SOC	Battery state of charge [%]	*rms*	Root-mean square
T	The total time period	*serv*	Service
V	Voltage [V]	t	t-th time interval
b	BESS operating variable [‘0’ discharge, ‘1’ charge]	*T*	Terminal

I. INTRODUCTION

Emission regulations imposed by the international marine organization (IMO), along with growing concerns on the environment, are causing a major shift in the industry’s approach to propulsion system design and increasing the demand for environmentally friendly marine power system solutions [1, 2]. In addition, the fluctuation of oil prices required the incentive to investigate more technologically advanced and efficient solutions to reduce operational expenses in the transportation industry [3, 4]. Therefore, the industry has collectively been exploring other opportunities for emissions control and energy savings which range from burning low emission fuels such as liquefied natural gas [1] and using dual fuel [5] to progressively electrify ships through increasing hybridization [6]. In the same context, the IMO suggested the concept of hybrid electric vessels as one of the energy efficient index to control and limit a vessel’s emissions [7]. This has opened up the integration of energy storage systems (ESSs) and renewable energy sources (RESs) into ship power systems [8, 9].

As the overwhelming majority of present electric vessels use AC distribution systems, the hybridization of ship power systems is complex as synchronization of each generation unit is required. In addition, ship AC distribution systems have drawbacks such as inrush current of transformers, three-phase imbalances, harmonic currents, and reactive power flow [10]. On the other hand, a DC distribution system provides an efficient distribution of electric energy by linking AC and DC energy sources through power-electronic devices which customize energy flow to the load [11, 12]. However, power electronic converters add complexity to the system due to their non-linear characteristics and switching behavior [13, 14]. Nevertheless, the recent progressive developments of power electronics devices make them more reliable and efficient. This makes the DC distribution is more feasible in various applications [12]. Therefore, the use of a HPS with DC distribution enables easier integration of RESs and ESSs [10, 15]. In addition, synchronization of generation units is not required which enables the prime movers to operate at their optimal speeds providing a reduction of fuel consumption and emissions [10, 16]. This also offers further advantages, such as space and weight savings, flexible arrangement of equipment and noise reduction from a diesel gen-set (DG) in the harbor [17, 18]. Moreover, retrofitting of a conventional marine power system with emerging renewable energy and energy storage technologies provides significant cost and environmental benefits [9, 19, 20]. As a result, the transition from a ship power system with AC distribution to a HPS with DC distribution is gaining more attention [12, 17].

The aforementioned advantages of a HPS with DC distribution give an efficient power system solution for short-haul ferries as most ferries operate closer to urban areas where the reduction of noise and emissions is required [21]. As most of the ferries use fossil fuels such as diesel to produce on-board power, they produce pollutant emissions, include CO_2, NO_X, SO_X and particular matter [22, 23]. When a ferry is berthed at a terminal, these emissions occur close to human habitation and result in a more direct impact on health [24]. Moreover, ferries account for a significantly high percentage of in-port emissions based on frequencies of calls compared to other types of vessels [25]. Such greenhouse gas emissions have a significant risk on human health including chronic bronchitis, heart disease, stroke and respiratory tract infection [22]. Therefore, policy makers have explored and introduced several methodologies in limiting port

emissions based on port structural changes [26, 27]. A cold-ironing method can be considered as a common solution to reduce in-port emissions and noise at terminals [28]. This method uses shore power to supply power to the on-board engines [29]. However, sometimes the shore power supply uses non-renewable energy sources [30]. In addition, economic factors need to be taken into account to justify investment in a shore power station as short-haul ferries usually berth for short period [28]. Therefore, there should be a more reliable solution to eliminate in-port emissions from ferries. Thus, all-electric and hybrid-electric ferries are practically achievable and the integration of RESs greatly reduces their emissions and fuel consumption. However, the slow dynamics or intermittent nature of RESs prevents them being the main source of power in ferries. Thus, a battery energy storage system (BESS) has become an integral part in such systems to ensure a reliable supply of power [31]. Therefore, the trend towards integration of the BESS into ferries has gained more attention in recent years. For example, MV Hallaig, the first hybrid electric ferry with battery storage, started operation in 2013 recording significant fuel savings and emission reductions [32]. Following the same trend in fuel and emissions reduction, Ampere ferry, the first battery powered ferry in the world, started operation in 2015 and reported a significant fuel savings with zero emission operation [17, 21, 33]. This trend is continuing as more ferries are being built with hybrid and fully battery powered systems owing to their advantage of emission reductions, especially as most ferries operate close to human habitation areas [11, 21, 32, 33].

The DC HPS with a BESS can be considered a promising solution to reduce emissions and noise in harbors to significantly low levels. In order to increase the potential of such a system, an efficient power management strategy is essential which can optimally share power among all HPS components. In this context, modeling a simulation platform is vital to derive an efficient power sharing strategy and thereby achieve fuel savings and emission reductions. Power and size optimization approaches for land-based HPSs have been extensively discussed [34, 35]. However, modeling, simulation and power management optimization of electric ferries with HPSs have not been extensively discussed. Only a few studies have discussed the use of HPSs in domestic ferry and boat applications, which mostly used classical and deterministic PMS methods [36-41]. In [36], the authors have studied and designed a hybrid fuel cell electric propulsion system for a domestic ferry and compared it with the performance of the existing diesel propulsion system. In [37], the development and demonstration of a fuel cell/battery hybrid system for a tourist boat is presented. In [38], the authors have investigated the effectiveness of using a hybrid system with battery in a passenger ferry. In [39], the authors proposed a hybrid fuel cell/battery power system for a low power boat. A classical energy management system, namely a state-based method, is used to manage the power generation. In [40], authors proposed an energy management system based on a deterministic state-based control method to manage the energy of a hybrid fuel cell/battery passenger ferry. In [41], the authors presented a techno-economic approach to minimize the overall cost of an ESS in a supercapacitor plug-in ferry. The aforementioned studies have not considered modeling, simulation, and evaluation of a hybrid domestic ferry with DC distribution and a BESS in terms of fuel savings and emission reductions. Moreover, to the best of our knowledge, the power management of DC HPSs for short haul ferries integrated with a BESS using a meta-heuristic method has not been reported in the existing literature.

The contributions of this paper can be summarized as follows:

- Performance comparison of using a hybrid DC over a conventional AC power system for short-haul ferries in terms of fuel consumption and emissions reductions;
- An approach to estimate the fuel consumption through the SFOC of a diesel engine;
- Optimal management and exploitation of generation and BESS for fuel consumption, greenhouse gas emissions and in-port noise reductions;
- Design, application and comparison of classical (RB method) and meta-heuristic (GWO) power management methods to optimally manage the power generation in hybrid ferries.

In order to examine and validate the proposed HPS system, a measured load profile of an existing ferry in Tasmania, Australia, is used.

The paper is organised as follows. The performance indicators used to evaluate the proposed system and PMS are presented in section II. The PMSs used in this study to optimally manage the power of the hybrid ferry are presented in section III. Modelling of the the proposed system components is given in section IV. The case study used and the corresponding proposed HPS are presented in section V. Results of the simulation and analysis are presented in Section VI to demonstrate the effectiveness of HPS over AC system for short-haul ferry application. Finally, conclusions drawn from the results of this study are given in Section VII.

II. PERFORMANCE INDICATORS

A. Fuel consumption

The presence of dynamic loads in marine power systems makes marine diesel engines operate at changing conditions. As a result, engines are not operated at their optimum loading conditions which in turn increases the fuel consumption

[42]. SFOC is a measure of the fuel efficiency and fuel savings of any prime mover that burns fuel and produces power [43]. An SFOC curve can be used to identify the optimum operating region of a given engine and thereby take measures to improve the fuel consumption. Typically, the optimum loading range for diesel engines is within 60% to 100% of the rated engine power [44]. Operating the engine in this range will significantly reduce the SFOC to lower levels.

The SFOC can be used to estimate the fuel consumption of the on-board engines. Several methods are available in the literature to estimate the fuel consumption of marine engines [43, 45, 46]. Generally, these methods are used to estimate the fuel consumption and emissions of main and axillary engines of large marine vessels with long voyages and several route options. In this context, recognized values of SFOC and emissions factors are essential to estimate the fuel consumption and emissions [47]. Under those circumstances, the traffic emissions assessment model (STEAM2) is used to estimate emissions and fuel consumption of a ship's main and axillary engine [43]. In a STEAM2 model, several data inputs are required such as ship speed, load profile, ship movement engine loads and fuel changes. Three relative SFOC for medium and large size engines provided by manufacturers were used. It was found that the relative SFOC curve of all three engines has the parabolic shape as shown in Fig. 1. This results in the conclusion that minimizing fuel oil consumption and improving the performance of engines can be achieved by running the engines at high engine loads.

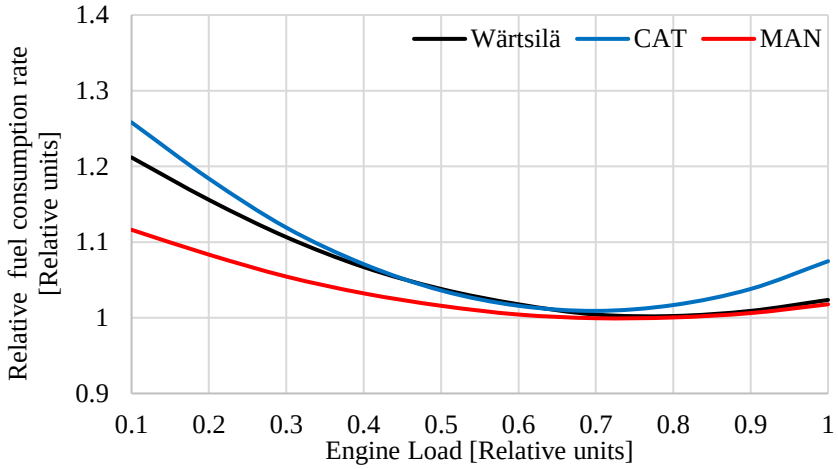

Fig. 1. The relative SFOC based on data of three manufacturers: Wärtsilä, Caterpillar and MAN [43]

In this paper, a simple approach to estimate the fuel consumption for short-haul ferries is proposed. The proposed approach is similar to [43] in some aspects. However, in this approach, the SFOC in L/kWh is estimated rather than using a relative SFOC. In addition, in this approach, only the load profile is required to estimate the SFOC which is then used to calculate the fuel consumption of the engine. The applicability of the proposed approach is validated through a real case study described in section V.

The fuel consumption in L/h at different engine loads is extracted from the manufacturer's data sheet [48]. The SFOC (L/kWh) curve shown in Fig. 2 is derived by dividing the fuel consumption at each engine load by the rated engine power (kW).

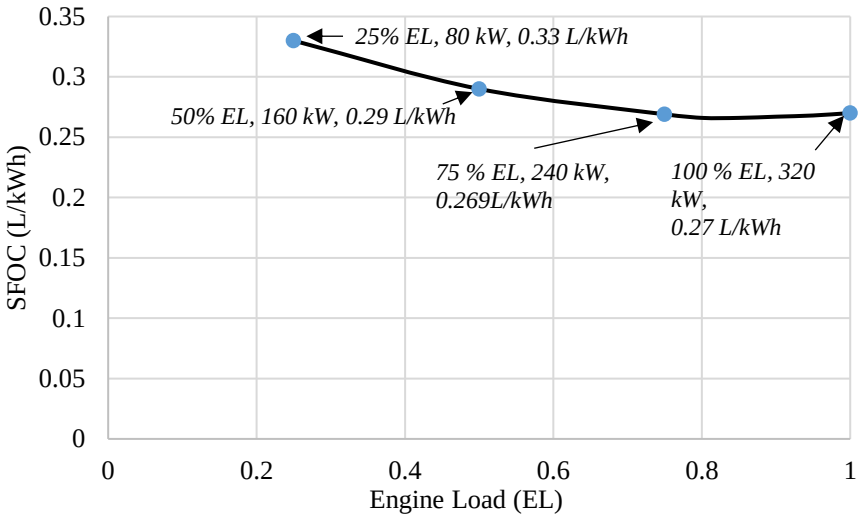

Fig. 2. The SFOC curve of the 320 kW Cummins Gen-Set (Model C350 D6)

The parabolic shape of the SFOC curve shown in Fig. 2 can be represented by a second degree polynomial function (quadratic function):

$$y = a\,x^2 + b\,x + c \tag{1}$$

Where *a*, *b* and *c* are the coefficients of the equation, *x* is the engine load and *y* is the SFOC.

By using regression estimation, the coefficients of the second degree polynomial equation for the SFOC are calculated and presented in Table 1.

Table 1. The coefficients of the SFOC equation

Coefficient	a	b	c
Value	0.1691	-0.2924	0.3929

Therefore, the derived quadratic equation for the SFOC can be expressed as:

$$SFOC = 0.1691\,EL^2 - 0.2924\,EL + 0.3929 \tag{2}$$

Where EL is the engine load expressed by:

$$EL = \frac{Generated\ Power\ (kW)}{Engine\ Rated\ Power\ (kW)} \qquad ; 0 \leq EL \leq 1 \tag{3}$$

The total fuel consumption in liters (FC_{total}) of the ferry for a complete round trip is the summation of fuel consumption at each operating condition:

$$FC_{total} = FC_{berth} + FC_{cruising} \tag{4}$$

Where FC_{berth} is the fuel consumption when the ferry is berthed (at terminal) and $FC_{crusing}$ is the fuel consumption when the ferry is cruising.

The fuel consumption in liters at any operational mode can be calculated by:

$$FC_m = SFOC_{EL}(P_{EL} \times t_m) \tag{5}$$

Where *m* represents the ferry operation mode (berth or cruising), $SFOC_{EL}$ is the value of SFOC at a specified engine load, P_{EL} in the instantaneous generated power at the specified engine load, and t_m is the time duration in hours at the specified engine load.

B. Emission reductions

Emission reduction is an important factor in maritime transportation. Many inventories have been introduced to calculate and estimate emissions from marine vessels [47, 49]. Generally, estimation is based on activity and/or fuel consumption. An activity-based approach requires detailed data such as ship speed, engine workload, routing, location,

time information, ship profile and duration [50, 51]. Therefore, the activity-based approach is generally used to estimate the emissions from large ships [51]. A fuel-based approach is a top-down method to estimate emissions based on fuel consumption. In this approach, the fuel consumption/energy consumption is required to estimate emissions [51]. This paper uses the Entac inventory with the top-down method, as it covers the emissions estimations from ferries and requires only the load profile of the engine to calculate the emissions [52]. In this method, the CO_2, SO_X and NO_X emissions are estimated as a function of the vessel energy consumption multiplied with an emission factor at each operating condition [51, 53]. Table 2 provides the equations used in estimating the emissions [52].

Table 2. Emissions estimation equations (summarized from [52])

	CO_2 emissions, e_{CO2} (g/kWh)	SO_X emissions, e_{SOX} (g/kWh)	NO_X emissions, e_{NOX} (g/kWh)
Berth	682 x output energy	11.6 x output energy	12 x output energy
Cruising	620 x output energy	10.5 x output energy	15 x output energy

III. POWER MANAGEMENT STRATEGY (PMS)

A power management unit is essential in order to optimally reduce the operating hours of the diesel engines, run the engines at their maximum efficiency and maintain the battery state of charge (SOC) at a certain level. In this paper, deterministic control method, namely rule-based (RB) control strategy, and a meta-heuristic on-line optimization method, namely Grey Wolf Optimization (GWO), are proposed and implemented. Fuel consumption and emission reductions are used as indictors to investigate the performance of each method.

A. Rule-based (RB) strategy

This strategy uses pre-determined operational conditions (states) to control the power sharing among the two diesel-generator sets (DGs) and the BESS. The advantages of this deterministic RB method are a low computational burden on the processor and relatively simple implementation [54]. Nevertheless, there can be performance degradations as it uses pre-determined states which could vary over time [40, 55].

Several operating states based on battery SOC and total load power are defined in order to control the power sharing of each component. The flow chart of the proposed RB PMS is shown in Fig. 3. The input variables are battery SOC and total load power (P_L). Outputs are the decisions to switch the DGs on/off and charge/discharge the BESS. When the SOC is within the lower boundary ($SOC^{min} \leq SOC < SOC^{high}$) and the load power exceeds a certain limit (P_L^{min}), the DG starts to supply power and shuts down as soon as the SOC exceeds the upper limit (SOC^{high}). During low power demand ($P_L \leq P_L^{min}$) when the ferry is at berth, the BESS operates in discharge mode to supply the load demand and both DGs are shut down. During medium power demand ($P_L^{min} < P_L \leq P_L^{ave}$), only one DG operates and the BESS is either charging or discharging depending on the SOC value. At high load demand ($P_L > P_L^{ave}$), both DGs operate and the BESS is either at standby mode or at charging mode depending on the value of SOC.

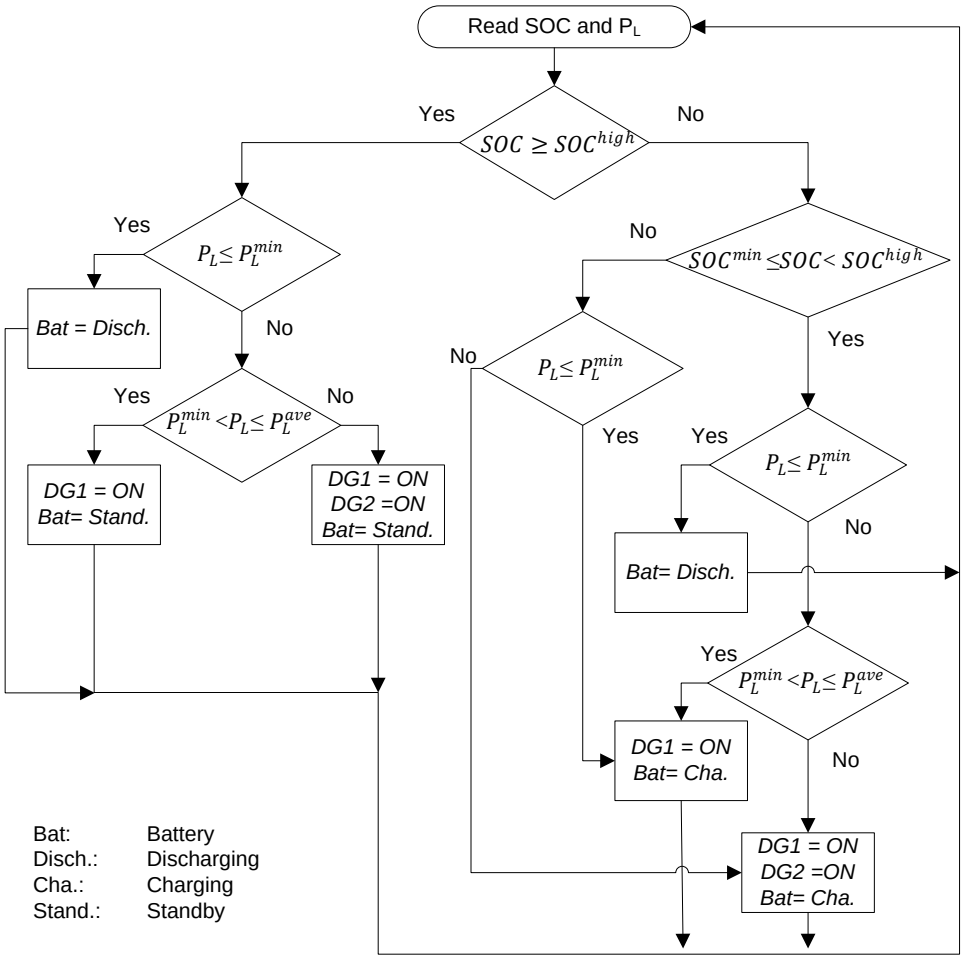

Fig. 3. Flowchart of the proposed rule-based (RB) PMS

B. Grey Wolf Optimization (GWO)

The use of meta-heuristic optimization techniques has gained huge attention over the last two decades. This is due to their capability of solving multi-objective optimization problems with several constraints. This provides better quality results compared to classical optimization techniques [34]. In this context, a meta-heuristic optimization technique, namely Grey Wolf Optimization (GWO), is implemented. The GWO is a population-based meta-heuristic swarm intelligence technique. This optimization technique was proposed in 2014 by Mirjalili [56]. Several studies have implemented GWO and compared its results with other algorithms. These studies found that GWO provides competitive optimization results compared to other swarm and evolutionary algorithms such as particle swarm optimization (PSO) [56-58], differential evolution (DE) [56], gravitational search algorithm (GSA) [56, 57], genetic algorithm (GA) [58] and ant colony optimization (ACO) [59].

This algorithm mimics the social behavior of the grey wolf. Grey wolves live and hunt in groups of 5 to 12 individuals. The social hierarchy of the grey wolves is represented in Fig. 4. The highest level of the hierarchy contains the leader of the wolf pack, represented as alpha (α). The leader is responsible for making decisions to hunt, wake and sleep. The second level in the hierarchy is called beta (β). These wolves are considered as consultants to the α wolf which are considered as the second best wolves in the pack. They convey the orders to the lower level wolves and send feedback of low level wolves to α wolf. The third level wolves are called delta (δ). They obey instructions from the α and β wolves. The lowest level in the hierarchy is omega (ω) wolves and their role is only to follow the orders of the higher-level wolves.

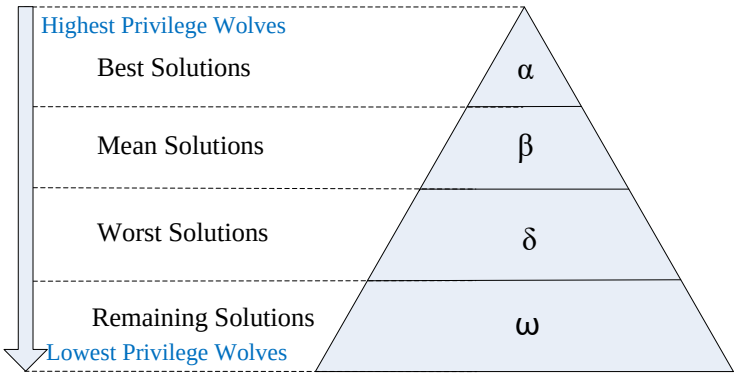

Fig. 4. The social hierarchy of grey wolves

One of the important social activities of grey wolves is hunting. The steps of this process include: (i) tracking, chasing and approaching the prey, (ii) pursuing, encircling and harassing the prey; and (iii) attacking the prey [56]. In order to mathematically represent the social hierarchy and hunting technique of grey wolves α is considered as the best solution, β the second best solution (mean solution), δ is the third best solution (worst solution) and ω is the other solutions. The first step in hunting is encircling the prey. The equations of this behavior are [56]:

$$D^{\rightarrow} = \left|C^{\rightarrow}.X_p^{\rightarrow}(\mathrm{t}) - \mathrm{X}^{\rightarrow}(t)\right| \quad (6)$$

$$X^{\rightarrow}(t+1) = X_p^{\rightarrow}(t) - A^{\rightarrow}.D^{\rightarrow} \quad (7)$$

Where $D^{\rightarrow}$ is a calculated vector used to specify a new position of the wolf, $\mathrm{X}^{\rightarrow}$ is the position vector of the wolf, and $X_p^{\rightarrow}$ is the position of the prey $A^{\rightarrow}.D^{\rightarrow}$ are coefficient vectors calculated by [56]:

$$A^{\rightarrow} = 2a^{\rightarrow}.r_1^{\rightarrow} - a^{\rightarrow} \quad (8)$$

$$C^{\rightarrow} = 2.r_2^{\rightarrow} \quad (9)$$

Where $a^{\rightarrow}$ is a vector set to decrease linearly from 2 to 0 over the iterations and $r_1^{\rightarrow}$ and $r_2^{\rightarrow}$ are random vectors in [0,1].

As mentioned earlier, only the alpha wolf guides the hunting process. Therefore, it is considered the best solution. Beta and delta wolves are participating and assisting in the hunting process. Therefore, alpha, beta and delta are considered as the three first solutions. Then the other search agents update their positions according to the best search agents. The new position vector of each wolf is calculated by the following equations [56]:

$$D_{Alpha}^{\rightarrow} = \left|C_1^{\rightarrow}.X_{Alpha}^{\rightarrow} - X^{\rightarrow}\right| \quad (10)$$

$$D_{Beta}^{\rightarrow} = \left|C_2^{\rightarrow}.X_{Beta}^{\rightarrow} - X^{\rightarrow}\right| \quad (11)$$

$$D_{Delta}^{\rightarrow} = \left|C_3^{\rightarrow}.X_{Delta}^{\rightarrow} - X^{\rightarrow}\right| \quad (12)$$

$$X_1^{\rightarrow} = \left|X_{Alpha}^{\rightarrow} - A_1^{\rightarrow}.D_{Alpha}^{\rightarrow}\right| \quad (13)$$

$$X_2^{\rightarrow} = \left| X_{Beta}^{\rightarrow} - A_2^{\rightarrow}.D_{Beta}^{\rightarrow} \right| \quad (14)$$

$$X_3^{\rightarrow} = \left|X_{Delta}^{\rightarrow} - A_3^{\rightarrow}.D_{Delta}^{\rightarrow}\right| \quad (15)$$

$$X^{\rightarrow}(t+1) = \frac{X_1^{\rightarrow}+X_2^{\rightarrow}+X_3^{\rightarrow}}{3} \quad (16)$$

Where $\mathrm{D}_{\mathrm{Alpha}}^{\rightarrow}$, $\mathrm{D}_{\mathrm{Beta}}^{\rightarrow}$ and $\mathrm{D}_{\mathrm{Delta}}^{\rightarrow}$ are calculated vectors used to specify new positions of the wolf, $\mathrm{X}_{\mathrm{Alpha}}^{\rightarrow}$, $\mathrm{X}_{\mathrm{Beta}}^{\rightarrow}$ and $\mathrm{X}_{\mathrm{Delta}}^{\rightarrow}$ are the vectors of the grey wolf's positions, and $X_1^{\rightarrow}$, $X_2^{\rightarrow}$ and $X_3^{\rightarrow}$ are the position vectors of the wolves.

Alpha, beta and delta wolves estimate the possible positions of the prey while the simulation is running. The alpha solution is used as a final solution as it always provides the optimal (best) solution-set compared to beta and delta.

1) GWO application on a hybrid electric ferry

The GWO tool is used to solve the power management optimization of the short-haul hybrid ferry. The main objective function of the optimization is to minimize the fuel consumption of DG1 and DG2. The optimization parameters are the DG1 power, DG2 power and battery power. Optimizing these parameters will optimize the value of SFOC and results in reduction of fuel consumption and emissions. The DG1 and DG2 powers are optimized based on running at least one DG at the optimal operating point and ensuring that the other DG is operated above the low operational efficiency region. This can be achieved by uniformly charging the battery in order to keep the engine operating at highest engine load over the entire cruising period. In addition, fuel consumption minimization includes shutting down the DGs at low load demand (at terminal) as DGs are required to operate only at higher load demand. This operation will eliminate the noises (in addition to emissions elimination) at terminal as both DGs are not operating. Therefore, emissions and noise reductions at berth (terminal) are then incorporated in the fuel consumption minimization. The main objective function of the fuel consumption minimization is presented as follow:

$$FC_{total} = \sum_{t=1}^{\mathrm{T}} \sum_{n=1}^{\mathrm{N}} (SFOC_n . P_{tn} . g_{tn} . \Delta t) \tag{17}$$

Where FC_{total} is the total fuel consumption of the ferry (L), P_{tn} is the power generated by n-th DG at t-th time (kW), g_{tn} is the DG operating variable (0 is "OFF" or 1 is "ON"), Δt is the time step, *t* is t-th time interval, *N* is the number of DGs and $SFOC_n$ is the specific fuel oil consumption of n-th DG represented by the following equation,

$$SFOC_n = \left[a \left(\frac{P_{tn}}{P_{rated}} \right)^2 - b \left(\frac{P_{tn}}{P_{rated}} \right) + c \right] . (P_{tn} \times t) \tag{18}$$

Where a,b and c are the coefficients of the SFOC equation and P_{rated} is the DG rated power (kW).

The optimization objective function is subjected to the following constraints:

- *Power balance constraint*

The power supplied from the generation side must be equal to the load demand for any period *t,*

$$\sum_{t=1}^{\mathrm{T}} \sum_{n=1}^{\mathrm{N}} \left(P_{tn} + P_{B,t} \right) = P_{L,t} \tag{19}$$

Where $P_{B,t}$ is the BESS power at t-th time (kW) and $P_{L,t}$ is the load power at t-th time.

- *Power constraints of DG units*

The power generated from each DG must be within the allowable limit

$$P_n^{min} \leq P_n \leq P_n^{max} \tag{20}$$

Where P_n is the power generated by n-th generator (kW), and $P_n^{min}$and P_n^{max} are the minimum and maximum power limit of the DGs (kW).

- *BESS constraints*

The battery power must be within the allowable limit. The maximum and minimum power of the BESS is determined based on the battery datasheet and complying with the load profile. These limits can be obtained by proper sizing of the BESS based on the measured load profile. The BESS constraints are as follow:

$$P_B^{min} \leq P_B \leq P_B^{max} \tag{21}$$

$$P_{dcha}^{min} \leq P_{dcha} \leq P_{dcha}^{max} \tag{22}$$

$$P_{cha}^{min} \leq P_{cha} \leq P_{cha}^{max} \tag{23}$$

$$E_B^{min} \leq E_B \leq E_B^{max} \tag{24}$$

$$SOC^{min} \leq SOC \leq SOC^{max} \tag{25}$$

Where:

$$P_{B,t} = P_{dcha,t} \times (1 - b_t) - P_{cha,t} \times b_t \quad (26)$$

$$P_{dcha,t} = \frac{P_{L,t}}{\eta_{dcha}} \quad ; P_{L,t} \leq P_{cha}^{max} \quad (27)$$

$$P_{cha,t} = \left(1 - \frac{E_{B,t_c}}{E_B^{max}}\right) \times P_{cha}^{max} \times \eta_{cha} \quad ; P_{L,t} > P_{cha}^{max} \quad (28)$$

$$E_{B,t} = E_{B,t-1} + \left[P_{dcha,t} \times (1 - b_t) - P_{cha,t} \times b_t\right].\Delta t \quad (29)$$

$$SOC_t = \left(\frac{E_{B,t}}{E_B^{max}}\right) \times 100\% \quad (30)$$

Where P_B^{min} and P_B^{max} are the minimum and maximum BESS power (kW), P_{dcha} and $P_{cha,t}$ are the discharging and charging power of the battery (kW), P_{dcha}^{min} and P_{dcha}^{max} are the minimum and maximum discharging power (kW), P_{cha}^{min} and P_{cha}^{max} are the minimum and maximum charging power (kW), E_B^{min} and E_B^{max} are the minimum and maximum BESS energy (kWh), SOC^{min} and SOC^{max} are the minimum and maximum state of charge of the BESS, η_{dcha} and η_{cha} are the discharging and charging efficiency of the battery, $E_{B,t}$ is the BESS energy at t-th time (kWh), b_t is the BESS operating variable at t-th time ['0' discharge, '1' charge], SOC_t is the BESS state of charge at t-th time,

P_{cha}^{max} is used as a threshold value to differentiate between load demand interval (usually at terminal) and high demand interval (usually while cruising). When the load demand is less than the maximum charging power ($P_{L,t} \leq P_{cha}^{max}$), the ferry is at the low demand interval (at terminal). When the load demand is more than the maximum charging power ($P_{L,t} > P_{cha}^{max}$), the ferry in at the high demand interval (cruising).

- *GHG emissions constraints*

The DGs are the GHG emissions source in the system. Therefore, the emissions constraints are designed to ensure that the emissions at terminal (berth) are always zero. The berth and cruising emissions are calculated based on Table 2.

$$e_{berth} = 0 \quad ; P_{L,t} \leq P_{cha}^{max} \quad (31)$$

$$e_{cruising} \leq e_{max} \quad ; P_{L,t} > P_{cha}^{max} \quad (32)$$

Where e_{max} is the maximum emissions limit in g/kWh (when both generators are operated at their maximum capacity), e_{berth} and $e_{cruising}$ are the emissions at berth (terminal) and while cruising calculated by the following equations:

$$e_{berth} = e_{CO_2}^{berth} + e_{SO_X}^{berth} + e_{NO_X}^{berth} \quad (33)$$

$$e_{cruising} = e_{CO_2}^{cruising} + e_{SO_X}^{cruising} + e_{NO_X}^{cruising} \quad (34)$$

Where $e_{CO_2}^{berth}$, $e_{SO_X}^{berth}$ and $e_{NO_X}^{berth}$ are the CO_2, SO_X and NO_X emissions at berth (g/kWh) and $e_{CO_2}^{cruising}$, $e_{SO_X}^{cruising}$, $e_{NO_X}^{cruising}$ are the the CO_2, SO_X and NO_X emissions while cruising (g/kWh).

- *Blackout prevention constraints*

Blackout prevention constraints are important to ensure reliability and security of the power system. The differences between the maximum power at generation side (including BESS) and the maximum load power must be more than or equal to zero.

$$N \times g_{tn} \times P_n^{max} + P_{B,t}^{max} - P_{L,t} \geq 0 \quad (35)$$

Where $P_{B,t}^{max}$ is the maximum power of the BESS at t-th time (kW) and it can be calculated by:

$$P_{B,t}^{max} = P_{dcha}^{max} \times (1 - b_t) - P_{cha}^{max} \times b_t \quad (36)$$

The GWO algorithm for fuel consumption minimization of the short-haul hybrid ferry has been implemented using MATLAB software. The GWO parameter values used during the simulation are maximum number of iterations = 1000,

number of search agents = 30 and problem dimensions is equal to three. The flowchart of fuel consumption minimization using GWO is shown in Fig. 5.

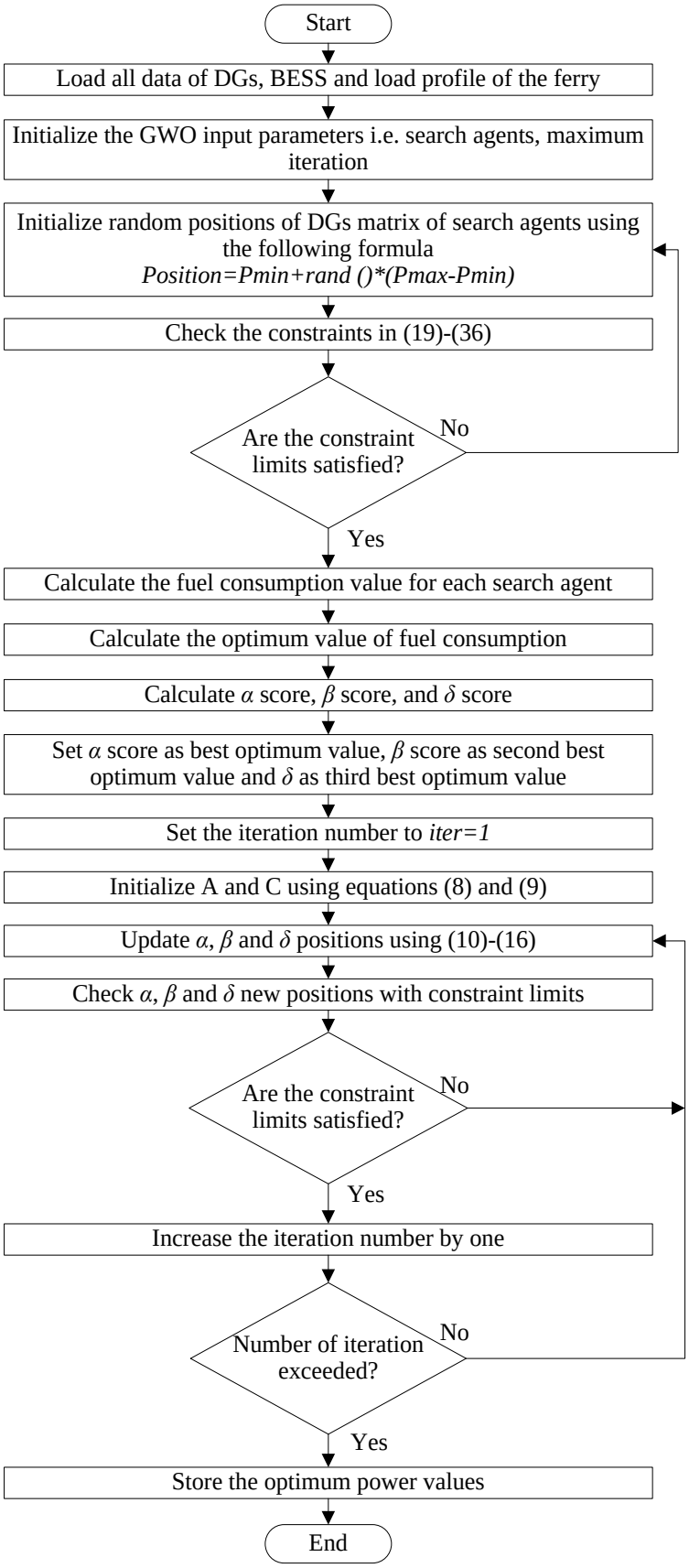

Fig. 5. Flowchart of the power management strategy using GWO

IV. SYSTEM MODELING

A. Loads

Usually the main load of a fixed route short haul ferry is the propulsion load while the service load takes a small portion of the total load. To simplify the model representation of the propulsion load, a variable resistance is used to represent the propulsion load. The load profile in kW is converted into a pure resistance values by the following equation:

$$R = \frac{V_{bus}^2}{P_L} \tag{37}$$

where V_{bus} is the measured voltage at the bus and P_L is the load power in kW.

The total resistance value of the load profile is distributed to the main load and secondary load. The main load is considered as a propulsion load as it is considered the largest load while the secondary load is the service load. The resistance distribution of the load profile can be calculated by:

$$R_{prop} = \lambda_p \, R \tag{38}$$

$$R_{serv} = \lambda_s R \tag{39}$$

where R_{prop} is the propulsion load resistance (Ω), R_{serv} is the service load resistance (Ω), λ_{prop} is the ratio of propulsion load and λ_{serv} is the ratio of service load.

B. Diesel Gen-Set (DGs)

Diesel generators are considered as the main power source in the vessel. The diesel generator specifications are used based on Cummins DG specifications [48]. Table 3 provides the technical specification of the existing DGs.

Table 3. Diesel set specifications (summarized from [48])

Generator specifications			
Model	C350 D6	Output power (kWe)	320
S rating (kVA)	400	Output voltage (V)	416
P.f	0.8	Phase	3
Frequency (Hz)	60		
Engine Specifications			
Manufacturer	Cummins	Model	NTA855 G3
Output – Prime (kWm)	358	No. of cylinders	6 in- line
Rated speed (rpm)	1800		

The synchronous round rotor machine is used to model the diesel generator. For simulation, transient and sub transient parameter values are converted to fundamental per-unit parameters based on classical definitions.

The synchronous machine equations are expressed with respect to a rotating reference frame defined by the equation

$$\theta e(t) = N_p \theta r(t) \tag{40}$$

where θ_e is the electrical angle, N_p is the number of pole pairs, and θ_r is the rotor angle.

The model of the diesel gen-set contains sub-models for the synchronous round rotor machine, speed governor and automatic voltage regulator. The governor, which comes as an electronic controller, regulate the diesel fuel supply to the engine which in turn control the rotational speed of the rotor(ω). The controller lets the frequency vary in proportion to the active power (P) of the load. The block diagrams of the droop speed controller is shown in Fig. 6.

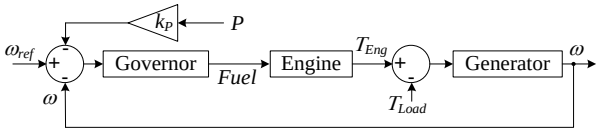

Fig. 6. Block diagram of the speed controller of the DG [60]

C. Battery Sizing

A BESS is used to reduce the diesel fuel consumption by supplying electricity to loads at low demand conditions at the terminal. The size capacity of the BESS is calculated by the following equation:

$$E_B = N_S E_{T,max} + 0.2 \times N_S E_{T,max} \tag{41}$$

$$E_B = N_S E_{T,max}(1 + 0.2) \quad (42)$$

Where E_B is the energy capacity of the battery pack in kWh, N_S is the number of stops per one round-trip and $E_{T,max}$ is the highest energy at one terminal in kWh. The constant 0.2 represents the minimum SOC (80% DOD) recommended from several marine battery manufacturers to maintain a reasonable cycle life of the battery [61, 62]. Looking into different marine battery manufacturers, the battery module specification shown in Table 4 is considered in this study [61].

Table 4. Battery module specifications

Manufacturer	Model	Cell Chemistry	Energy (kWh)	Capacity (Ah)	Voltage Range (V)			Max. discharge power P_{dcha}^{max} (kW)	Max. charging power P_{cha}^{max} (kW)	Cycle Life at 80% DoD
					Max	Nominal	Min			
PBES	Power 65	NMC	6.5	75	100	88.8	77	45	22.5	15000

The number of battery modules in the BESS is determined based on the total energy required. In other words, the total energy capacity of the battery pack must be larger than or equal to the maximum energy required by the load. The battery modules can be arranged into several different configurations depending on the voltage level and the current capacity required. The two common battery configurations are parallel and series configurations as shown in Fig. 7. The parallel configuration provides more current capacity (Ah) than series configuration. Hence, parallel configuration is used for high current low voltage applications while series configuration is applicable for low current and high voltage applications.

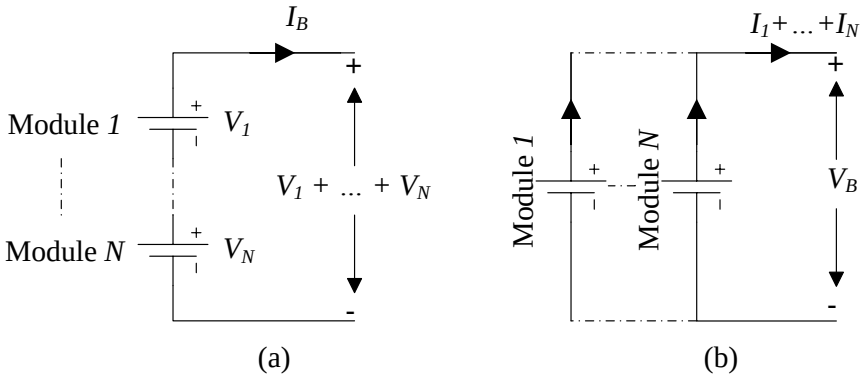

Fig. 7. Battery module configurations: (a) Series configuration and (b) Parallel configuration

D. Inverter

An inverter is used to convert the DC voltage from the DC bus to AC voltage at the required voltage level and frequency to drive the propulsion motors. A schematic diagram of the inverter is shown in Fig. 8.

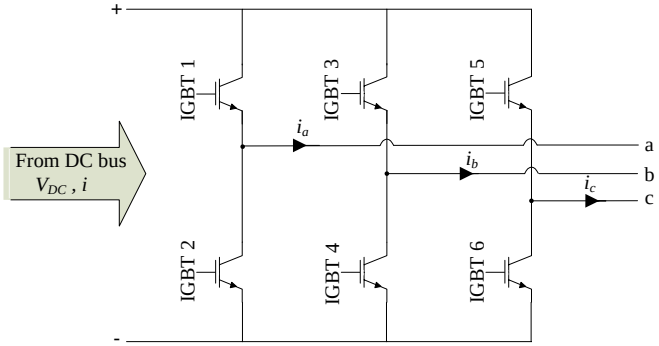

Fig. 8. The equivalent circuit of the average inverter

The power, resistance, and currents are defined by

$$P_{AC} = -v_a i_a - v_b i_b - v_c i_c \quad (43)$$

$$R_{DC} = \frac{v_{DC}^2}{P_{AC} + P_{fixed}} \quad (44)$$

$$i = \frac{V_{DC}}{R_{DC}} \tag{45}$$

where i_a, i_b, i_c are the respective AC phase currents flowing into the inverter, P_{AC} is the power output on the AC side, P_{fixed} is the fixed power loss that is specified on the block, R_{DC} is the resistance on the DC side, and i is the current flowing from the positive to the negative terminals of the inverter.

The ratio of V_{rms} to V_{dc} is chosen to be 0.7797 based on the following equation [63].

$$V_{rms}(line - line) = \frac{\sqrt{6}}{\pi} V_{DC} \tag{46}$$

E. Rectifier

The rectifier is used to convert three-phase AC voltage to DC voltage. The average rectifier model produce a full-wave output using the six-pulse rectifier. The schematic diagram of the six-pulse rectifier is shown in Fig. 9.

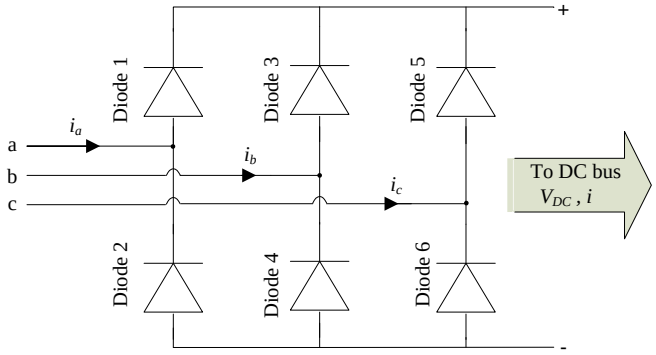

Fig. 9. The equivalent circuit of the average rectifier

The output voltage of the rectifier V_{dc} is:

$$V_{DC} = \frac{3\sqrt{2}}{\pi} \times V_{RMS} \tag{47}$$

where

$$V_{RMS} = \sqrt{\frac{(v_a - v_b)^2 + (v_b - v_c)^2 + (v_c - v_a)^2}{3}} \tag{48}$$

v_a, v_b, v_c are the respective AC input phase voltages.

The power into the rectifier is defined in the following equation:

$$P_{AC} = P_{loss} + P_{DC} \tag{49}$$

The DC power output from the rectifier is:

$$P_{DC} = P_{AC} - P_{loss} \tag{50}$$

The power loss drawn by the rectifier is:

$$P_{loss} = \frac{V_{Rated}}{R_{fixed}} \tag{51}$$

where V_{Rated} is the rated voltage at the AC side and R_{fixed} is the phase series resistance in an equivalent wye connected load.

F. DC-DC Converter

To incorporate the BESS to the HPS, a DC-DC converter is normally used. A behavioural model of a bidirectional DC-DC converter is used to regulate and convert the DC voltage of the battery from one voltage level to another. In addition, the converter is used to regulate and stabilize voltage at the dc bus. The output voltage of the converter is defined by:

$$v = v_{ref} - i_{load}D + i_{load}R_{out} \quad (52)$$

where v_{ref} is the DC bus voltage set point, and D is the value for the output voltage droop with an output current parameter.

The block parameters of the DC-DC converter are shown in Table 5.

Table 5. DC-DC converter block parameters

DC bus voltage reference (*Vref*)	520 V
Related output power	200 kW
Droop parameterization	By voltage droop with output current
Output voltage droop with output current	0.05
Power direction	Unidirectional
Maximum expected supply-side current	135 A

V. CASE STUDY

A. Description of ferry and voyage

Bruny Island is located off the south-eastern coast of Tasmania, Australia, and encompasses approximately 363 square kilometers; it is considered a popular tourist attraction. Access to Bruny Island is available by two ferries, namely Mirambeena and Bowen. In this paper, Bowen ferry is selected as the case study. Bowen ferry operates between Kettring (terminal 1) and Bruny Island (terminal 2) as shown in Fig. 10.

Fig. 10. The examined ferry route

The specifications of Bowen ferry are given in Table 6. The ferry operates six days a week and performs 42 round trips per week (7 round trips per day) during the peak period.

Table 6. Ferry specifications

Bowen ferry specifications and voyage descriptions					
Ferry capacity	Less than 30 vehicles	Service speed	7 knots	Length	35 m
Powering	2 x 400 kVA (320 kW)	Fuel type	Diesel	Breadth	15 m
Travel distance	6.2 km (round – trip)	Travel duration	60 minutes (round trip)	Propulsion	2 x Azimuth thrusters

The single-line diagram of the existing AC power system is shown in Fig.11. The model includes two DGs, propulsion loads and a service load.

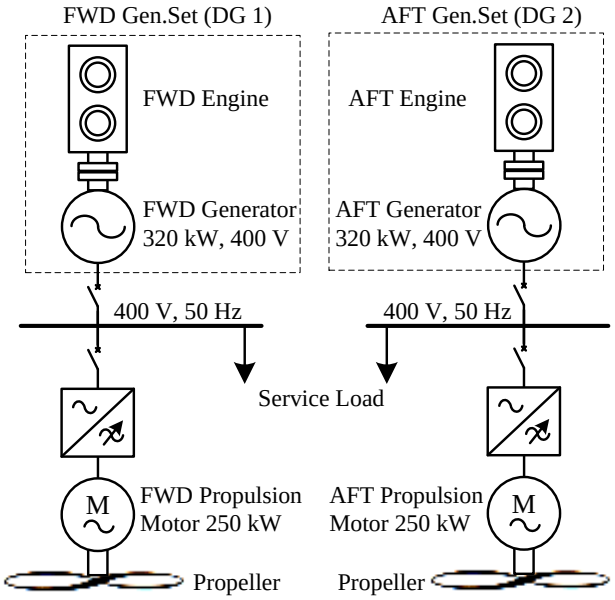

Fig. 11. Single-line diagram of the existing ferry power system

The measured load profile of the ferry is shown in Fig. 12.

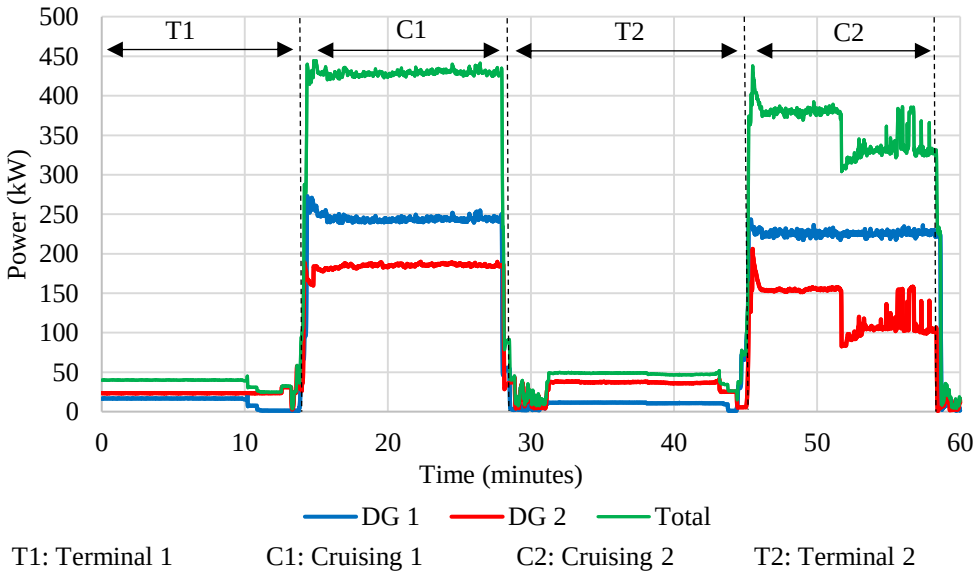

Fig. 12. The measured load profile of Bowen Ferry

According to the measured load profile, the ferry requires a total energy of 200.175 kWh to complete one round trip. The energy consumption for each operational condition is shown in Fig. 13. The energy consumption at terminal, which also covers the manoeuvring period, occurs below 67 kW, while energy consumption at cruising covering the manoeuvring period occurs above 67 kW. As this ferry is a single deck ferry, the wind effect is negligible. In addition, as the ferry is operated within an area enclosed by land (as this ferry is a short-haul ferry which operates for short distances only), the wave effect is also negligible. In the first cruising period, the ferry was fully loaded with the maximum vehicles capacity (30 cars). In the second cruising period, the load on the ferry was less than the first cruising period. As results, in the second cruising period, the thrusters require less power.

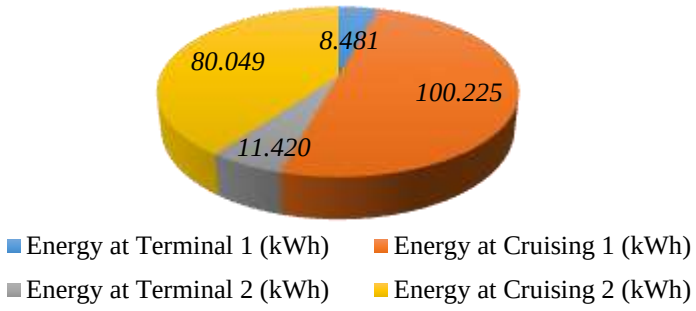

Fig. 13. The measured energy consumption for each operating condition

As mentioned in *section IV.A*, the load profile in kW is converted into a pure resistance value. The ratio of propulsion load to the total load λ_p is set to 0.9 while the ratio of service load to the total load λ_s is set to 0.1. Fig. 14 shows the voltage, current and resistance value of each propulsion load.

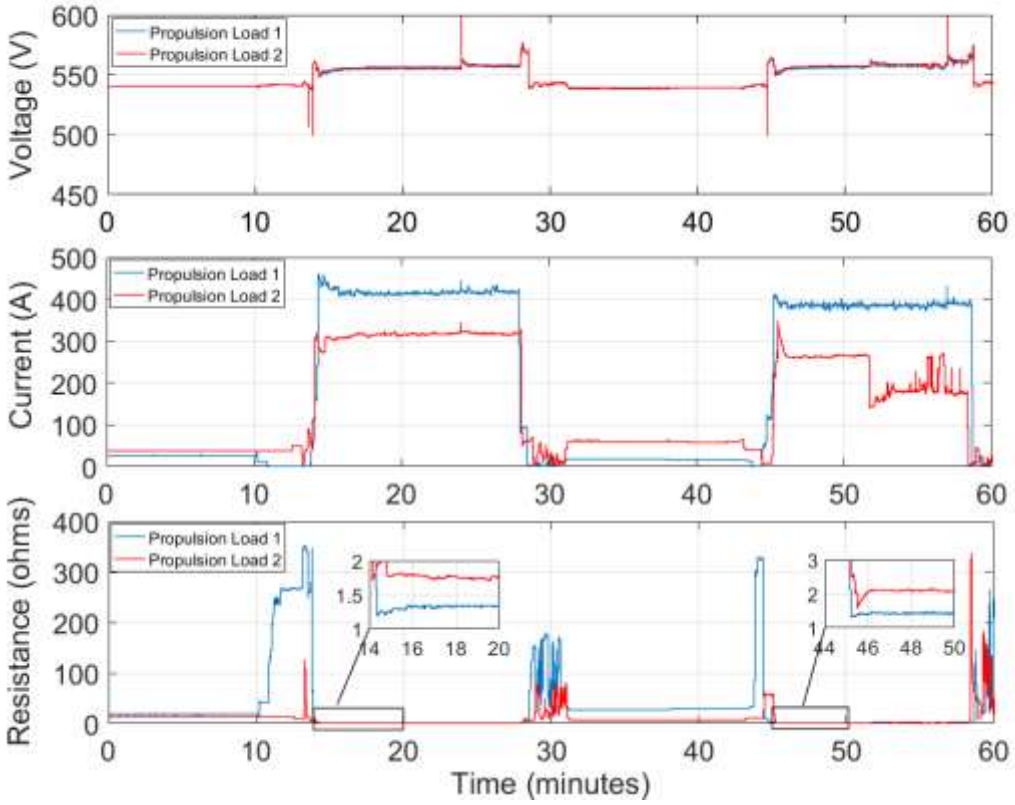

Fig. 14. Voltage, current and resistance of propulsion load 1 and 2

B. Proposed HPS with DC distribution

As the ferry terminal at Kettering is close to a residential area, emissions and noise produced by the on-board DGs is a concern. The emissions produced by the DGs cause direct impacts to the heath of people living near the ferry terminal. To overcome these issues, a BESS based HPS solution is proposed in this paper, where the engines are turned off when the ferry is in and around the terminals. For this purpose, the DC distribution system is proposed to replace the existing AC distribution system of the ferry. The single-line diagram of the proposed HPS with DC distribution is shown in Fig.15. The model includes two DGs, BESS, DC-DC converter, rectifiers, inverter, propulsion loads and service load.

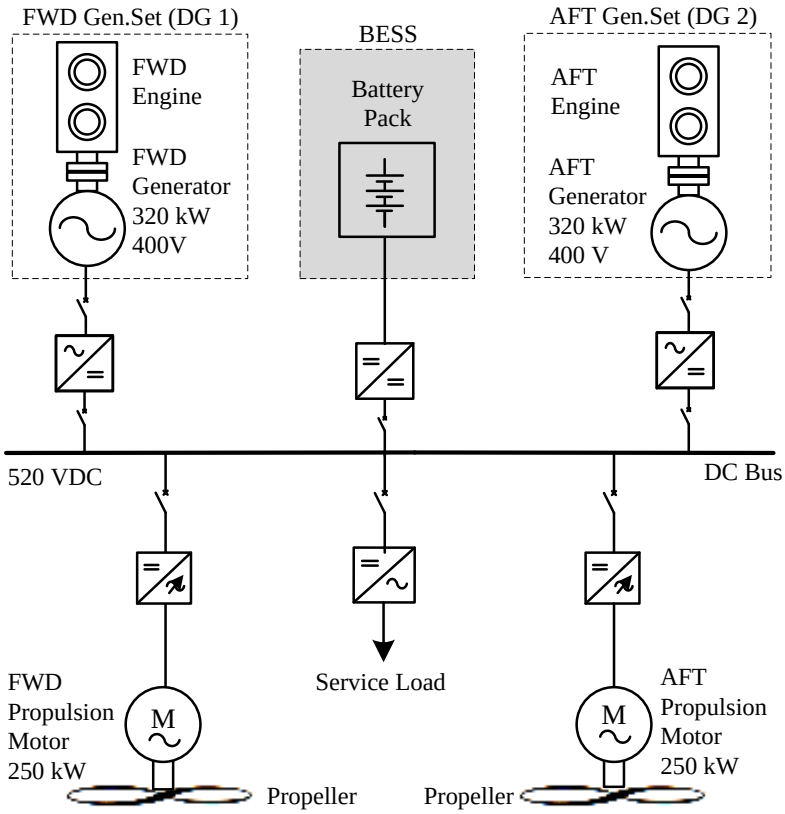

Fig. 15. The single-line diagram of the proposed HPS

The battery module specifications used for this case study are provided in Table 4. According to Fig. 12 and Fig.13, the maximum energy consumption ($E_{T,max}$) occurred at terminal 2. Therefore, $E_{T,max}$ is equal to the total energy consumption at terminal 2 which is 11.42 kWh.

By using equation (42), the total energy required from the BESS at berth is found to be 27.408 kWh. However, as there are two cruising periods in the one round trip, the battery pack can be charged in each cruising period. Therefore, the energy required from the battery pack can be reduced to half. As a result, the size capacity of the BESS can be 13.704 kWh. This will significantly reduce the initial cost of the battery system.

As the voltage at the DC bus is 520 V and the required energy capacity is low, the suitable configuration for the battery modules is the series configuration. Therefore, based on battery specifications provided in Table 4, three battery modules are considered to form the battery pack as shown in Fig. 16.

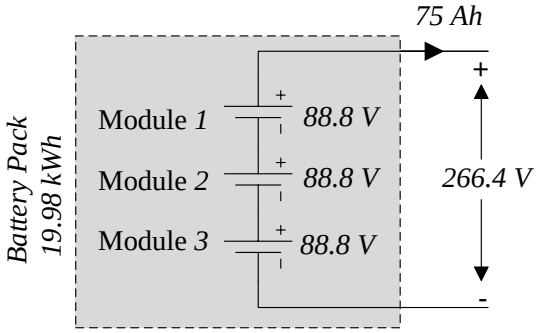

Fig. 16. Battery modules configuration in the battery pack

Based on the above, the specifications of the BESS pack are shown in Table 7.

Table 7. BESS parameters

Nominal Voltage (V)	Rated Current (Ah)	Energy Capacity E_B (kWh)	SOC (%)		Max. discharge power P_{dcha}^{max} (kW)	Max. charging power P_{cha}^{max} (kW)	Charge/Discharge Efficiency (%)
			Min	Max			
266.4	75	19.98	20	100	135	67.5	98

C. Fuel consumption indicator

Based on equation (2), the complete SFOC curve of the ferry's main engine is presented in Fig .17.

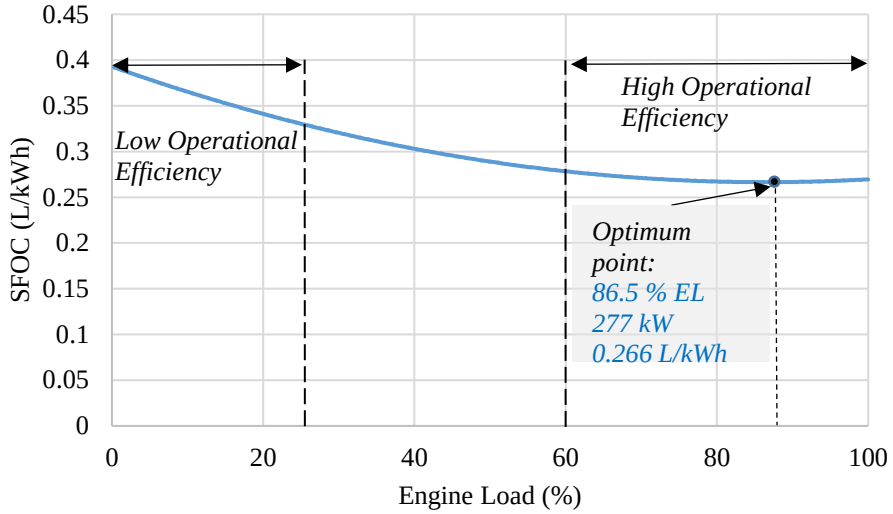

Fig. 17. The estimated SFOC curve of the existing diesel engine

DGs are generally considered as the main source of power in a hybrid ship power system. They provide continues supply which maintains the voltage and meets the average load demand. Whenever there are fluctuations in the load the BESS is used. To effectively run the diesel engine, it should operate only at its high operational efficiency range, that is from 60% to 100% of its rated power as shown in Fig 17. This attributes to lowering the fuel consumption of the diesel engine. As shown in Fig. 17, the optimal SFOC is 0.266 L/kWh at 86.5 % engine load. According to the proposed PMS, when the load demand is low, the BESS is operated as the main power supply source. This helps to lower the operating hours of the DGs which reduces fuel consumption, emissions and maintenance costs of the diesel generators, and increase fuel savings and the life time of the diesel generator. In addition, operating the BESS as the main power supply at low load demand (when ferry is at terminal) eliminates the noise from DGs.

Based on the measured power consumption profile and by using equations (2) - (5), the SFOC and fuel consumption for (DG 1) and (DG 2) are calculated and shown in Fig. 18.

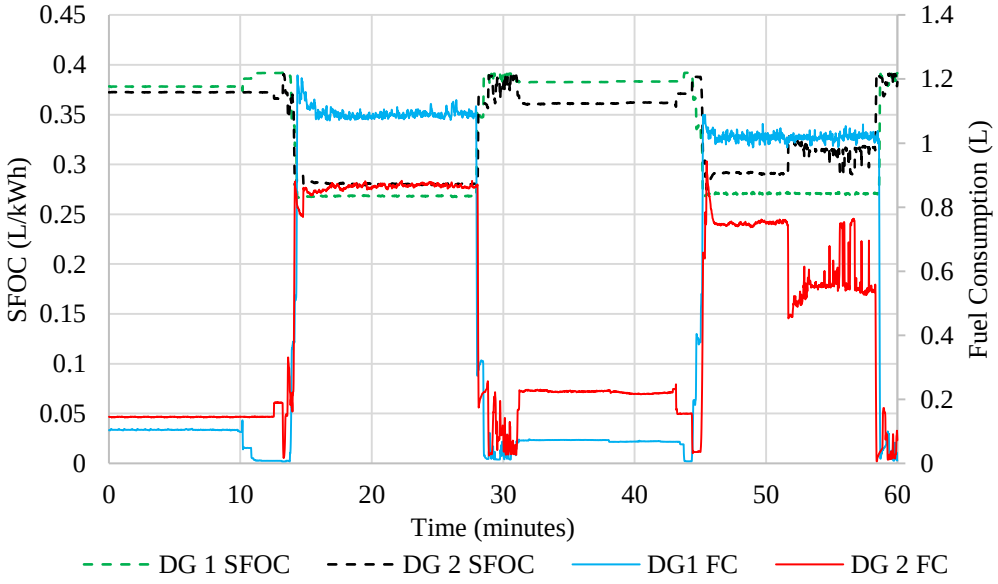

Fig. 18. SFOC and fuel consumption (FC) of DG 1 and DG2

The total fuel consumption of the ferry is 57.7 L, which consists of fuel consumption of DG 1 at 31.5 L and the fuel consumption of DG 2 at 26.6 L. Table 8 shows the fuel consumption for both engines at each terminal and at different operating conditions.

Table 8. The fuel consumption of each DG and total fuel consumption of the existing ferry

	Fuel consumption at berth (L)			Fuel consumption while cruising (L)			Total fuel consumption for complete round trip (L)
	At Terminal 1	At Terminal 2	At berth (T1 + T2)	While Cruising 1	While Cruising 2	While cruising (C1 + C2)	
DG 1	1.23	1.19	**2.42**	15.14	13.93	**29.07**	
DG 2	2.16	3.30	**5.46**	12.06	8.71	**20.77**	
Total	**3.38**	**4.49**	**7.87**	**27.20**	**22.63**	**49.83**	**57.70**

In order to calculate the fuel cost, the average price of diesel fuel of AUD$ 1.405 per liter in Tasmania is used (provided by the Australian Institute of Petroleum). Hence, the total fuel cost of one round trip is AUD$ 81.07.

D. Emissions indicator

In order to estimate the emissions produced by the ferry, measured energy consumption at berth and while cruising for the existing ferry system is used. Table 9 shows the CO_2, SO_X and NO_X emissions from the ferry per one round trip.

Table 9. The emissions produced by the ferry in one round trip

	CO_2 emissions, E_{CO2} (g/trip)	SO_X emissions, E_{SOX} (g/trip)	NO_X emissions, E_{NOX} (g/trip)	Total emissions (g/trip)
Berth	13572.48	230.85	238.81	14042.15
Cruising	111769.67	1892.87	2704.11	116366.65
Total	**125342.16**	**2123.73**	**2942.92**	**130408.80**

E. Ferry PMS parameters

The values used in the PMS of the proposed hybrid system are given in Table 10.

Table 10. PMS parameters of the proposed hybrid ferry

PMS parameters					
$SOC^{initial}$	100 %	P_{dcha}^{min}	0 kW	P_n^{min}	0 kW
SOC^{max}	100 %	P_{dcha}^{max}	135 kW	P_n^{max}	320 kW
SOC^{high}	90 %	P_{cha}^{min}	0	N	2
SOC^{min}	20 %	P_{cha}^{max}	67 kW	P_L^{max}	640 kW
P_B^{min}	-135 kW	E_B^{min}	3.996 kWh	P_L^{ave}	320 kW
P_B^{max}	67.5 kW	E_B^{max}	19.98 kWh	P_L^{min}	67 kW
η_{cha}	0.98	η_{dcha}	0.98	N_S	2

VI. Simulation Results And Analysis

The ferry takes 60 minutes to perform a complete round trip. The measured load profile is inserted into the MATLAB Simulink® simulation platform. The simulation of the existing AC system is performed to validate the model and estimate the SFOC, fuel consumption and emissions. Then, the HPS is simulated for same ferry operation with different PMSs to investigate the reduction of SFOC, fuel consumption and emissions compared with existing AC system. In addition, a performance comparison between classical and meta-heuristic PMSs used for the short-haul hybrid ferry is conducted.

A. Existing AC system

The existing AC system is modeled in Simulink. The measured load profile and the fuel consumption of the ferry are used to validate the accuracy of the simulation model.

From *section V.C*, the fuel consumption of the ferry based on the measured load profile is found to be 57.7 L. The simulation results of the model provided a total fuel consumption of 59.17 L as shown in Table 11. The error percentage between the calculated fuel consumption based on actual data and the simulated fuel consumption is 2.484 %. This percentage validated the accuracy of the simulation model.

Table 11. The comparison between the actual fuel consumption and the simulated fuel consumption

	Fuel Consumption of DG 1 (L)	Fuel Consumption of DG 2 (L)	Total fuel Consumption (L)
Calculated	31.5	26.2	57.7
Simulated	33.1	26.07	59.17
Total error (%)			**2.484**

The simulation outputs of generated powers from the two existing DGs and the load power are depicted in Fig. 19. The simulation results of the fuel consumption and generated powers show acceptable agreement between the measured load data and the simulated load profile from the model. This validated that the model is accurate with accuracy percentage of 97.516 %.

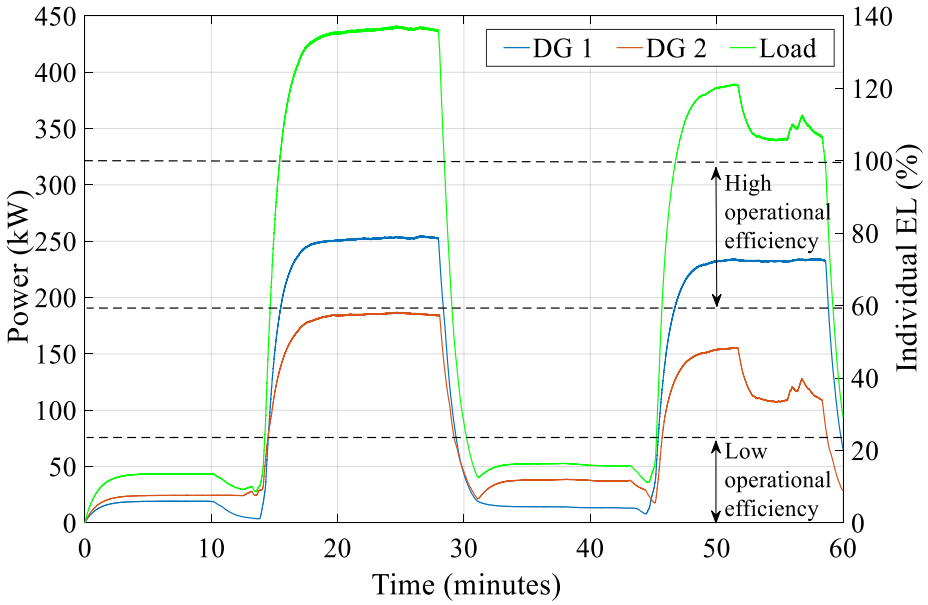

Fig. 19. Simulation output of power generated from diesel gen-sets

As can be seen from Fig. 19, both DGs are operated all the time. From 0 to 14 minutes and 30 to 45 minutes, the ferry is berthed at the terminal. The two DGs are operated to supply the load. In both periods, each DG is operated in the low operational efficiency range where each diesel engine generates approximately 20 kW (6.5 % of the engine rated load) in the period from 0 to 14 minutes and 25 kW (8.2 % of engine rated load) in the period from 30 to 45 minutes.

The simulation output of the fuel consumption when the ferry is berthed both at terminal 1 and 2 (FC_{berth}) is 8.43 L. Table 12 shows the fuel consumption obtained from the simulation model.

Table 12. The fuel consumption obtained from the simulation model

	Fuel consumption at berth (L)			Fuel consumption while cruising (L)			Total fuel consumption for complete round trip (L)
	At Terminal 1	At Terminal 2	At berth (T1 + T2)	While Cruising 1	While Cruising 2	While cruising (C1 + C2)	
DG 1	1.45	1.52	2.97	15.69	14.09	29.77	
DG 2	2.18	3.28	5.46	12.14	8.83	20.97	
Total	**3.62**	**4.80**	**8.43**	**27.83**	**22.92**	**50.75**	**59.17**

At the first cruising period from 15 to 29 minutes, DG 1 and DG 2 are operated at approximately 78 % and 57 % of rated engine load respectively. The corresponding fuel consumption during cruising period 1 ($FC_{cruising1}$) is about 27.83 L. At the second cruising period from 46 to 59 minutes, DG 1 operates at approximately 230 kW (71.8 % of rated engine load) while DG 2 operates from 155 kW to 107 kW (48.4 % to 33.4 % of rated engine load). The corresponding fuel consumption during cruising period 2 ($FC_{cruising2}$) is about 22.92 L. As a result, the total fuel consumption of both DGs while cruising ($FC_{cruising}$) is 50.57 L. Based on the simulation result, the fuel cost of one round trip is AUD$ 83.13.

From simulation results, the total energy required for one round trip is 202.903 kWh which consists of 20.98 kWh at berth and 181.93 kWh while cruising. The simulation results show acceptable agreement between the measured energy consumption, which is 200.175 kWh, and the simulated energy consumption, which is 202.903 kWh.

Based on the energy consumption output from the simulation model and the equations in Table 2, the CO_2, SO_X and NO_X emissions are calculated for both DGs and depicted in Table 13.

Table 13. The emissions obtained from the simulation model of the AC system

	CO_2 emissions, E_{CO2} (g/trip)	SO_X emissions, E_{SOX} (g/trip)	NO_X emissions, E_{NOX} (g/trip)
Berth	14306.27	243.33	251.72
Cruising	112794.20	1910.22	2728.89
Total	**127100.47**	**2153.56**	**2980.62**

B. HPS using Rule-Based method (HPS-RB)

The validated Simulink model of the existing AC system is then modified to the HPS with DC distribution as depicted in Fig.15. As the proposed system consists of multi energy sources (DGs and BESS), a PMS is essential to ensure optimal sharing and operation of the system. In this sub-section, the proposed HPS is simulated with RB method as the PMS. The simulation output of the power generated by DG 1 and DG 2, load power and BESS power are shown in Fig. 20 and the SOC of the BESS is shown in Fig. 21.

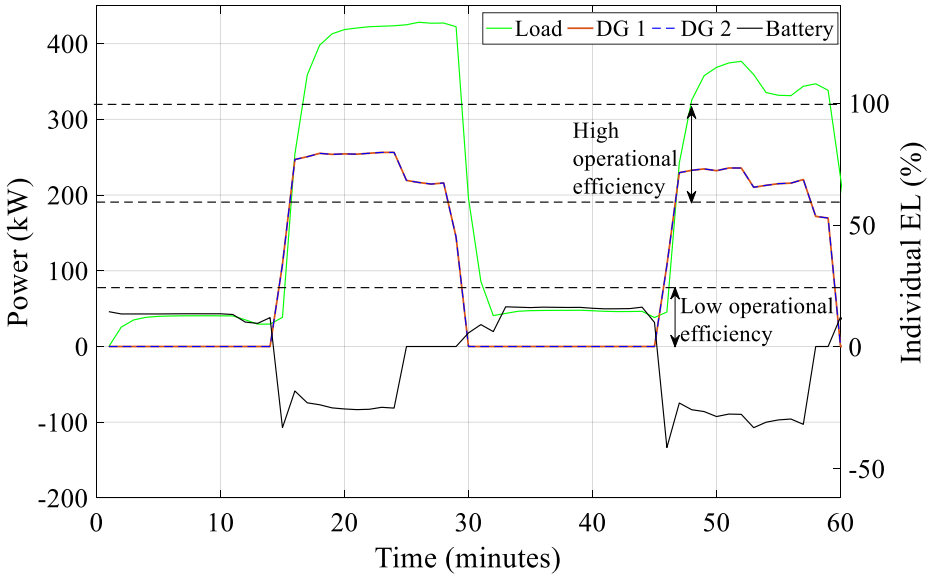

Fig. 20. The simulation output power of the proposed HPS-RB

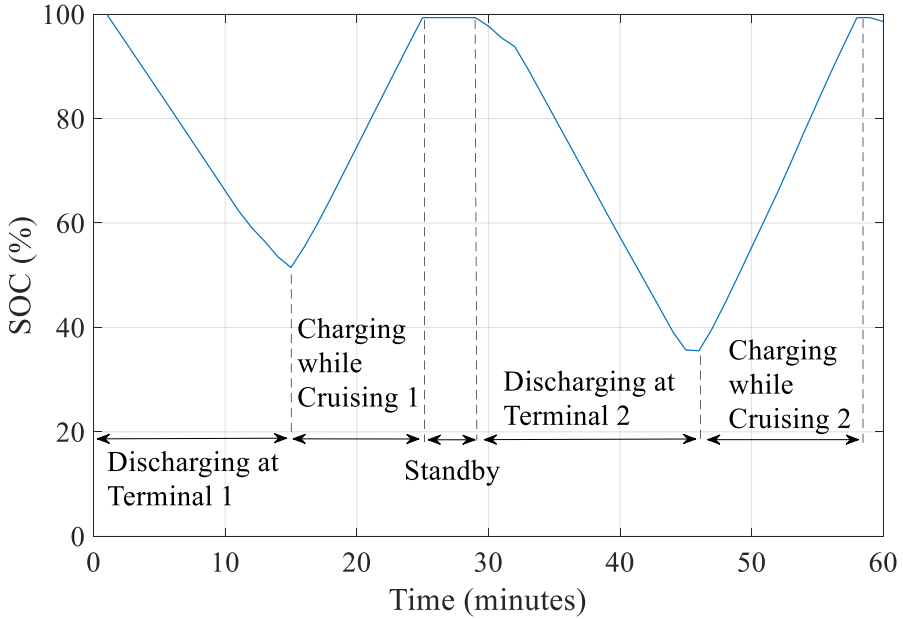

Fig. 21. The SOC of the BESS with HPS-RB

At the period from 0 to 14 minutes and 30 to 45 minutes, when the ferry is at the terminal, the load power is less than the lower load power boundary of the controller as shown in Fig. 20 and the battery SOC is at the upper boundary as shown in Fig. 21. Therefore, the controller disconnected both DGs and discharged the battery in order to supply the load demand. This provides quieter operation and zero emissions as the ferry is in the terminal and close to a residential area. As both DGs are disconnected at this period, the FC_{berth} is equal to zero.

At the first cruising period from 15 to 29 minutes, both DGs are running at their high operational efficiency range by generating 256 kW each. At this period, the battery SOC is at the low boundary limit as shown in Fig. 21. Therefore, the battery is in the charging mode. At t = 24, the battery starts to operate in standby mode as the battery's SOC reaches the allowable limit after the battery is being charged. As a result, the fuel consumption of the first cruising period $FC_{cruising1}$ is 30.74 L. At the second cruising period from 46 to 59 minutes, the controller connects both DGs and charges the battery as the load demand is increased and the battery SOC reaches the lower boundary. Each DG is operated at their high operational efficiency range by generating 236 kW to 210 kW (73.7% to 65.6 % of rated engine load). The controller is responsible for charging the battery only when both DGs are running at their high efficiency range and the battery SOC is at the lower boundary. Therefore, the battery is still charging, as the battery SOC has not reached a certain value set by the controller. At t = 58, the battery SOC reaches the allowable limit as shown in Fig.21. Due to that, the controller switches the battery to the standby mode. As a result, the fuel consumption in the second cruising period $FC_{cruising2}$ is 26.7. Therefore, the total fuel consumption of both DGs while cruising ($FC_{cruising}$) is 57.45 L. Overall, the total FC_{total} for one round trip (60 minutes) of the HPS using RB (HPS-RB) is 57.45 L. Table 14 shows the fuel consumption obtained from the simulation model of HPS-RB.

Table 14. The fuel consumption obtained from HPS-RB

	Fuel consumption at berth (L)	Fuel consumption while cruising (L)			Total fuel consumption for complete round trip (L)
		While Cruising 1	While Cruising 2	While cruising (C1 + C2)	
DG 1	0.00	15.37	13.35	28.72	
DG 2	0.00	15.37	13.35	28.72	
Total	**0.00**	**30.74**	**26.70**	**57.45**	**57.45**

The controller successfully achieves a good power sharing among the two DGs and BESS by operating both engines at their high efficiency range and discharges the battery at a low demand period when the ferry is at the terminal in order to reduce the fuel consumption and eliminate noise and emissions. However, as such classical PMS is set based on pre-determined conditions, the controller equally shares the power between DGs and runs them at their high operational range rather than optimal operation point. In addition, it is recommended to charge the battery at a lower charging rate in order to keep the power generated from DGs at the high operational range when the load demand decreases. For example, as shown in Fig 21, the battery is turned to standby mode at t = 25. This results in a reduction from 80 % to 67 % of engine load which results in a corresponding increment in SFOC from 0.26720 L/kWh to 0.2734 L/kWh. Therefore, it is recommended to charge the battery at a uniform charging rate over the complete cruising period to keep the diesel engines operating at a higher engine load.

The total energy consumption is found to be 210.67 kWh which is mainly occurred while cruising. The CO_2, SO_X and NO_X emissions are calculated for both DGs and depicted in Table 15.

Table 15. Emissions obtained from HPS-RB

	CO_2 emissions, E_{CO2} (g/trip)	SO_X emissions, E_{SOX} (g/trip)	NO_X emissions, E_{NOX} (g/trip)
Berth	0.00	0.00	0.00
Cruising	130614.67	2212.02	3160.03
Total	**130614.67**	**2212.02**	**3160.03**

C. HPS using Grey Wolf Optmization (HPS-GWO)

GWO is used to optimally manage the power sharing of the proposed HPS. As seen from the objective function of Eq. (17), the objective of optimization is to minimize the fuel consumption of DG1 and DG2 subject to the constraints explained in Eqs. (18)-(36). The main optimization parameters are the DG1 power, DG2 power and battery power. Optimizing those parameters will optimize the value of SFOC and results in reduction of fuel consumption. The power optimization results of the optimization parameters DG 1 power, DG 2 power and battery power are shown in Fig. 22 and the SOC of the BESS is shown in Fig. 23.

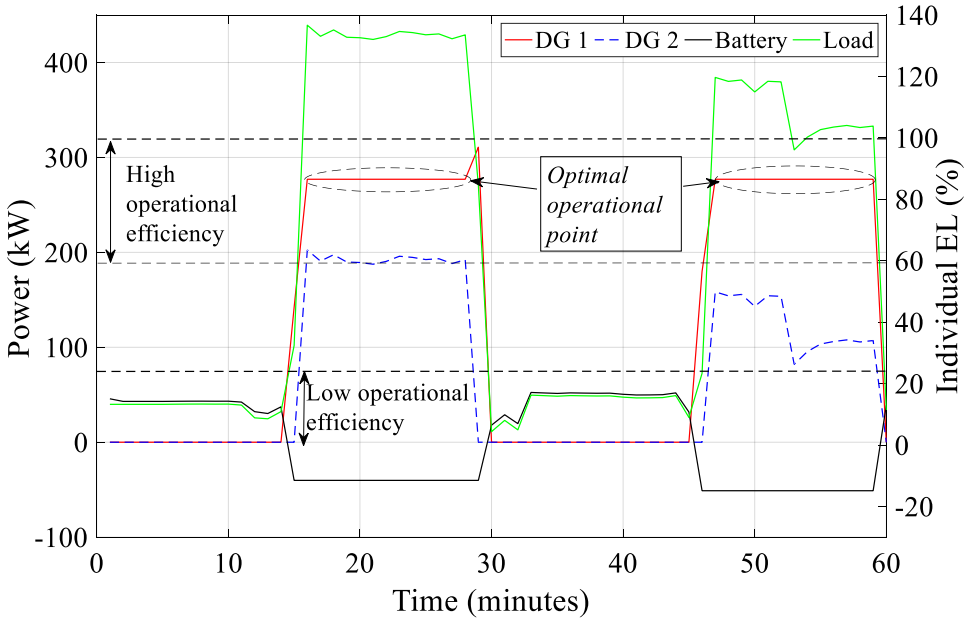

Fig. 22. The simulation output power of the proposed HPS-GWO

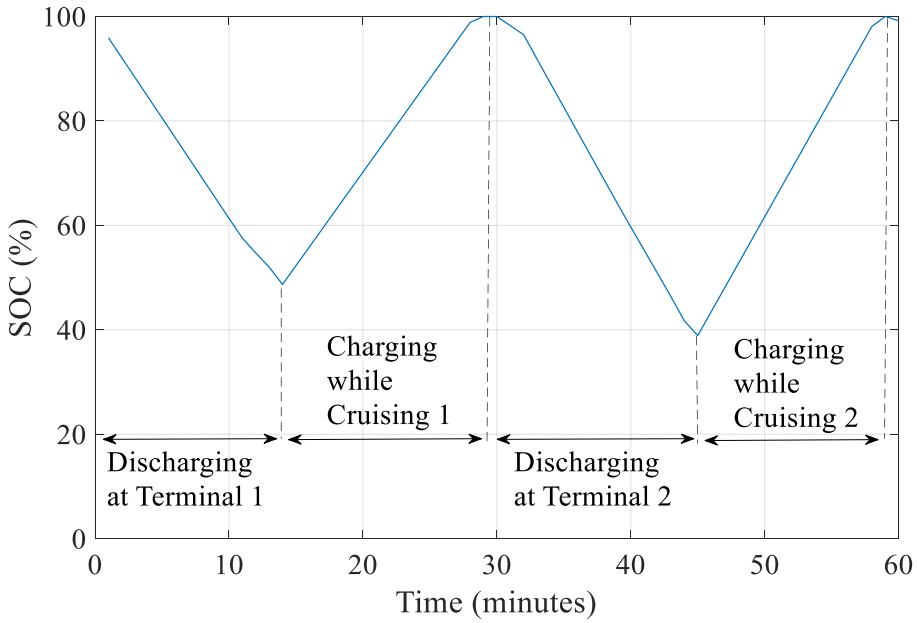

Fig. 23. The SOC of the BESS with HPS-GWO

At the period from 0 to 14 minutes and 30 to 45 minutes, when the ferry is at berth, the load power is less than the lower load power boundary and the battery SOC is at the upper boundary as shown in Fig. 23. Therefore, both DGs are off and the BESS is in the discharging mode. This provide quieter operation and zero emissions as the ferry is in the terminal and close to a residential area. As both DGs are disconnected at this period, the FC_{berth} is equal to zero.

At the first cruising period from 15 to 29 minutes, DG 1 is operated at its optimal operational point which is 86.5 % of engine load (277 kW). This results in a minimal SFOC of 0.266 L/kWh. In addition, DG 2 is maintained at approximately 58 % to 63 % engine load by uniformly charging the battery over the complete cruising period. As a result, the fuel consumption of the first cruising period $FC_{cruising1}$ is 29.70 L. At the second cruising period from 46 to 59 minutes, DG1 is also operated at its optimal operational point while DG2 is varying above the low operational efficiency range. This results in a fuel consumption of 25.05 L in the second cruising period. Therefore, the total fuel consumption of both DGs while cruising ($FC_{cruising}$) is 54.75 L. Overall, the total FC_{total} for one round trip (60 minutes) of the HPS with a GWO based power management strategy is 54.75 L. Table 16 shows the fuel consumption obtained by HPS-GWO.

Table 16. Fuel consumption obtained from HPS-GWO

	Fuel consumption at berth (L)	Fuel consumption while cruising (L)			Total fuel consumption for complete round trip (L)
		While Cruising 1	While Cruising 2	While cruising (C1 + C2)	
DG 1	0.00	18.09	16.84	34.93	
DG 2	0.00	11.61	8.21	19.82	
Total	0.00	29.70	25.05	54.75	**54.75**

The total energy consumption is found to be 201.142 kWh, which is mainly occurred while cruising. The CO_2, SO_X and NO_X emissions are calculated for both DGs and depicted in Table 17.

Table 17. Emissions obtained from HPS-GWO

	CO_2 emissions, E_{CO2} (g/trip)	SO_X emissions, E_{SOX} (g/trip)	NO_X emissions, E_{NOX} (g/trip)
Berth	0.00	0.00	0.00
Cruising	124707.73	2111.99	3017.12
Total	**124707.73**	**2111.99**	**3017.12**

D. Comparison

The main optimization parameters are powers of DG1, DG2 and battery. These parameters are optimized in order to keep the SFOC of the engine at optimal operational point and above low operational efficiency region. This results in fuel consumption reduction. The effect of those parameters on the SFOC and hence the fuel consumption of engine are summarized below.

Effects of the DG powers (DG1 and DG2) on the SFOC: As per Eq. (2) and corresponding Fig. 17, the increase of the generated power from the DG reduces the SFOC value until a certain point (optimal point) then it starts to increase slightly with the increase of DG power. Fig. 17 depict the effect of the variation of engine load (DG power) on the SFOC. As shown in this Fig. 17, the optimal SFOC point is 0.266 L/kWh at 86.5 % engine load (277 kW) which falls in the high operational efficiency region. In the high operational efficiency region, the maximum SFOC increment compared to the optimal point is 4.51 %. In the low operational efficiency region, the maximum and minimum SFOC are 0.391 L/kWh and 0.330 L/kWh at 1 % and 25 % engine load respectively (3.2 kW and 80 kW). In this region, the maximum and minimum SFOC increment compared to the optimal point are 46.99 % and 24.04 % respectively. Therefore, optimizing the power output of DG will results in more fuel consumption reduction.

Effects of battery power on SFOC: The battery is used to supply power when the ferry operated at low demand (at terminal). The use of the battery as a main power supply at terminal will reduce the total fuel consumption and eliminate emissions and noises as both DGs are not operating. At cruising periods, when the battery is charging, the power of the battery is optimized in the way that it gets charged in a uniform rate of charge. This will increase the load on the on-board DGs which will make the DGs operate at higher engine load over the complete cruising period. This will results in operating the engines above the low efficiency region over the entire cruising period which results in minimizing the SFOC and hence the fuel consumption.

The results of the SFOC and fuel consumption using RB method and GWO method compared to the existing AC system are shown in Fig. 24 and Table. 18. In the existing AC system, both DGs are operated at all times. As it can be seen from Fig. 24, both DGs are operated at low engine load at terminal 1 and 2. This attribute to significant increase in the SFOC. The results show that the proposed HPS using RB and GWO method provide 100 % reduction of SFOC at terminals (at berth) as both DGs are switched off and the BESS supplies power to the load. This results in a quiet operation (no noise from the DGs as both are switched off) and eliminates emissions at the terminal which is close to a residential area. In addition, as shown in Fig. 24, DG1 and DG2 produce same SFOC by using RB method, as both DGs are equally share the load power. In contrast, by using GWO method, DG1 always operates at optimal SFOC while DG2 is dealing with the load variation above the low operational efficiency range. Moreover, the operating hours of DG2 is reduced by three minutes compared to RB method.

The fuel consumptions in liters of each system are summarized in Table 18. With the HPS-RB, the fuel consumption of the DGs is reduced by 2.91 % despite that the energy consumption of the DGs being increased in order to charge the BESS. This is due to the fact that both DGs are not operated at their optimal operational efficiency level. With the HPS-GWO, more fuel consumption reduction is achieved with a percentage of 7.48 % and additionally the energy consumption of the DGs is reduced since DG 1 is always operated at its optimal point and DG 2 is always operated near its high operational range. Table 18 shows the summary of fuel consumption for each system.

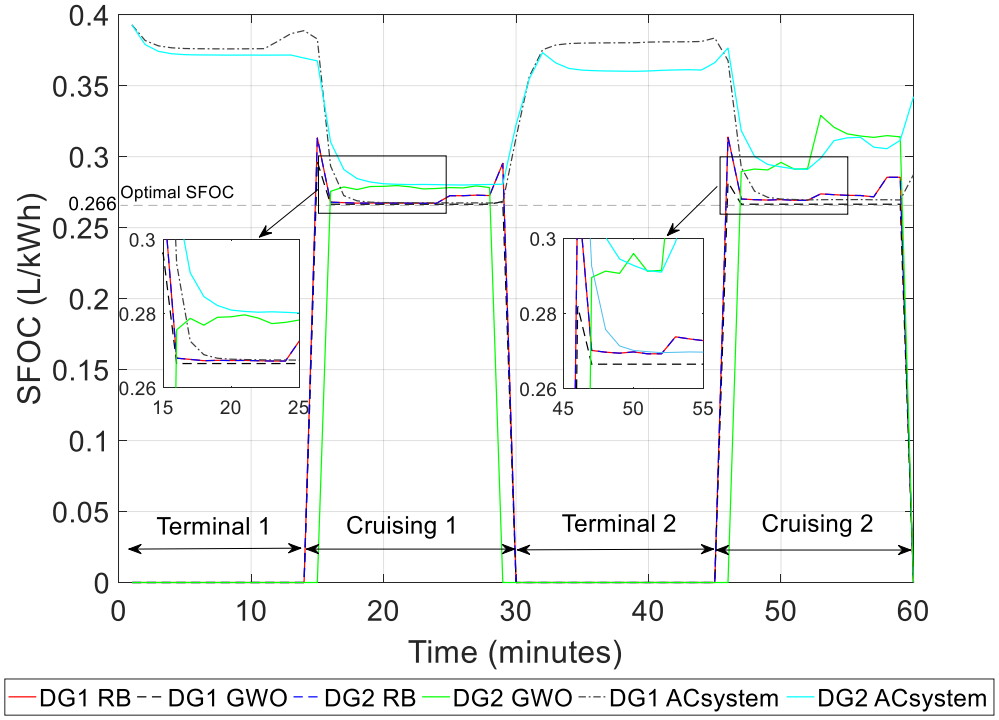

Fig. 24. SFOC results of the AC system and the proposed HPS using RB and GWO method

Table 18. Fuel consumption comparison among the three systems for one round trip

	Fuel consumption at Berth (L)	Fuel consumption while Cruising (L)	Total Fuel consumption for one round trip (L)	Fuel consumption reduction (L)	Fuel costs (AUD$)	Fuel savings (AUD$)	**Fuel consumption reduction (%)**
Existing AC system	8.43	50.75	59.17	-	83.133	-	-
HPS-RB	0.00	57.45	57.45	1.72	80.717	2.146	**2.91**
HPS-GWO	0.00	54.75	54.75	4.43	76.923	6.21	**7.48**

According to Table 18, there is a slight increment of fuel consumption in the proposed systems during cruising compared to the existing AC system. This is due to the extra power generated by the engines to charge the BESS. The HPS-GWO provided lower fuel consumption in the cruising period compared to the HPS-RB. This is due to the operation of DG 1 at its optimal operational point and eliminating the operation of DG 2 in the low operational range. This is done by uniformly charging the battery while cruising. On the other hand, as RB method uses a pre-determined condition to control the system, the HPS-RB runs both DGs at the same engine load by equally dividing the load power between both DGs. Overall, the HPS-RB and HPS-GWO provided 57.45 L and 54.75 L of fuel consumption respectively. The fuel consumption of each power system at different ferry operating conditions is shown in Fig. 25.

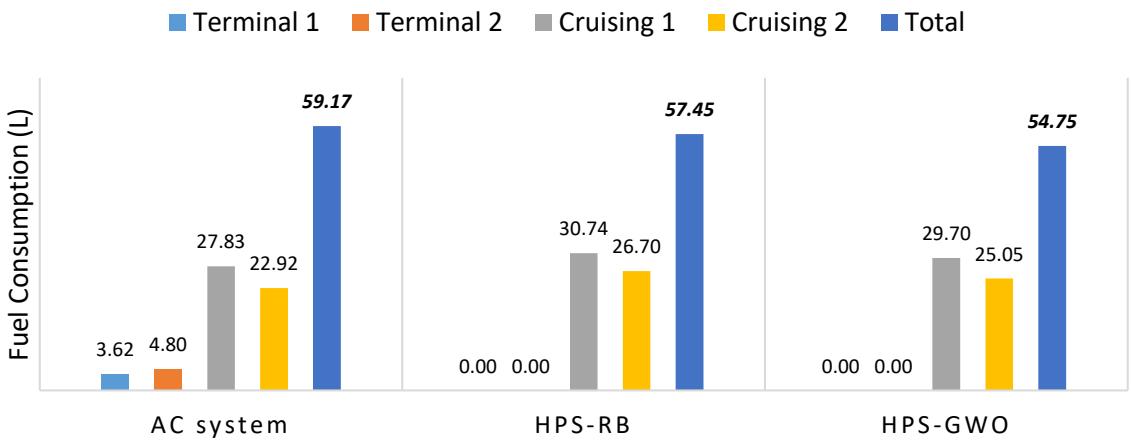

Figure 25. Fuel consumption comparison of each power system

The results show that the HPS provides a zero-emissions solution at berth. The energy consumption for each operating condition is used to calculate the emissions. The total energy consumption for the existing AC system, HPS-RB and HPS-GWO is 202.9 kWh, 210.67 kWh and 201.14 kWh respectively as shown in Fig. 26.

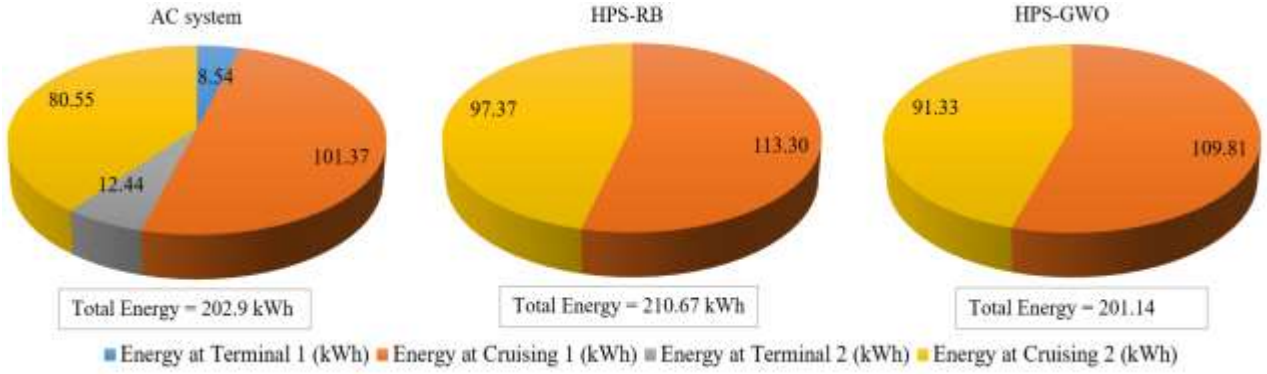

Fig. 26. Energy consumption of DGs for each system at different operating conditions

The proposed HPS with BESS provided a 100 % emissions reduction at terminal using both power management methods as shown in Table 19. Therefore, such HPS with BESS provide an efficient solution to eliminate berth emission for short-haul ferries that operate close to urban areas where the reduction of emissions is required to reduce the direct impact of emissions on human health. However, in the cruising period, the HPS-RB provide a 15.79 % and HPS-GWO provide 10.56 % increment in CO_2, SO_X and NO_X. This is due to the increase of the DGs' energy production to charge the on-board battery while cruising. In the HPS-RB, the CO_2, SO_X and NO_X emissions increase by 2.76 %, 2.71% and 6.01% respectively. In contract, in the HPS-GWO, CO_2 and SO_X emissions are reduced by 1.88% and 1.93 % respectively with slight increment of NO_X emission by 1.22 %.

Table 19. The emissions produced from each system for different operating conditions

	Emissions at berth (g/trip)			Emissions while cruising (g/trip)			Emissions for a complete voyage (g/trip)		
	CO_2	SO_X	NO_X	CO_2	SO_X	NO_X	CO_2	SO_X	NO_X
AC system	14306.27	243.33	251.72	112794.20	1910.22	2728.89	127100.47	2153.56	2980.62
HPS-RB	0.00	0.00	0.00	130614.67	2212.02	3160.03	130614.67	2212.02	3160.03
HPS-GWO	0.00	0.00	0.00	124707.73	2111.99	3017.12	124707.73	2111.99	3017.12
Reduction using HPS-RB	100 %	100 %	100 %	-15.79 %	-15.79 %	-15.79 %	-2.76 %	-2.71 %	-6.01 %
Reduction using HPS-GWO	100 %	100 %	100 %	-10.56 %	-10.56 %	-10.56 %	1.88 %	1.93 %	-1.22 %

VII. CONCLUSIONS

The DC-HPS with BESS can be considered as a promising solution to reduce the fuel consumption and thereby reduce the emissions in ferries. In order to optimally share the power among all HPS components in such complex systems, an

efficient power management strategy (PMS) is essential. This paper highlights the advantage of using a HPS with DC distribution and BESS over an AC power system for a short-haul RORO ferry. Two PMSs, namely RB and GWO, are proposed and implemented on the proposed HPS system. Performance comparisons of the two PMSs are carried out based on two evaluating indicators: fuel consumption and emissions reductions. The MATLAB/Simulink software is used to model and simulate the system. A case study with measured load profile of a short-haul RORO ferry is used to validate and examine the proposed system.

Simulation results showed that both methods, the HPS-RB and HPS-GWO, provide a 100 % reduction in fuel consumption at berth and a 2.91 % and 7.48 % reduction respectively during the complete voyage. A greater reduction is achieved with HPS-GWO as it operates the DG 1 at its optimal operational point and avoids running the DG 2 in the low operational range. This is achieved by uniformly charging the BESS while cruising, in order to maintain the engine performance at highest engine load over the entire cruising period.

In terms of emissions, the simulation results showed that the HPS-RB and HPS-GWO offer 100 % emissions reductions at berth. In the cruising period, the HPS-RB provide a 15.79 % and HPS-GWO provide 10.56 % increment in CO_2, SO_X and NO_X. This is due to an increase in the DGs' energy production to charge the on-board battery during cruising. However, the HPS-GWO provide 1.88 % and 1.93 % reduction of CO_2 and SO_X emissions respectively with 1.22 % increment of NO_X in the complete voyage.

Overall, the BESS integration into a short-haul ferry power system can be considered as an effective solution to reduce emissions and noise at the berth. This provides fuel consumption reductions as diesel engines' operating hours are reduced since they are shut down at the berth. In terms of power system architecture, a HPS with DC distribution is considered an effective architecture when incorporating an ESS into a ferry power system. This is due to system flexibility in operating each diesel engine at different speeds. For the PMSs, a meta-heuristic on-line optimization method, GWO, provides better fuel consumption and emissions reductions compared to a classical RB method which uses pre-determined conditions. This is due to the capability of GWO in solving multi objective optimization problems with several operational constraints to find the optimal solution in contrast to classical methods that use pre-determined conditions. Taken together, these results suggest that the DC - HPS with the BESS and the GWO-based power management strategy is a good combination to achieve low fuel consumption, low emissions and eliminate noises at berth for short-haul hybrid electric ferries. The insight gained from this study can be of assistance to marine coastal vehicles operating in close proximity to residential areas where both noise and air emissions are of concern.

Future work is required to develop a hybrid optimization method by combining two or more optimization techniques for more accurate and promising optimization results. In addition, studies could be extended to compare the performance of GWO with other meta-heuristic optimization for power management optimization of electric ferries. Moreover, recommendations for repetitive shutdown-restart of the engines should also be considered in the overall assessment of the proposed system. Research incorporating local controller with each component could also be conducted to improve the operation of the optimizer.

REFERENCES

[1] G. A. Livanos, G. Theotokatos, and D.-N. Pagonis, "Techno-economic investigation of alternative propulsion plants for Ferries and RoRo ships," *Energy Conversion and Management,* vol. 79, pp. 640-651, 2014.

[2] R. F. Nielsen, F. Haglind, and U. Larsen, "Design and modeling of an advanced marine machinery system including waste heat recovery and removal of sulphur oxides," *Energy Conversion and Management,* vol. 85, pp. 687-693, 2014.

[3] I. Shancita, H. H. Masjuki, M. A. Kalam, I. M. Rizwanul Fattah, M. M. Rashed, and H. K. Rashedul, "A review on idling reduction strategies to improve fuel economy and reduce exhaust emissions of transport vehicles," *Energy Conversion and Management,* vol. 88, pp. 794-807, 2014.

[4] G. G. Dimopoulos, C. A. Georgopoulou, I. C. Stefanatos, A. S. Zymaris, and N. M. P. Kakalis, "A general-purpose process modelling framework for marine energy systems," *Energy Conversion and Management,* vol. 86, pp. 325-339, 2014.

[5] P. García Valladolid, P. Tunestål, J. Monsalve-Serrano, A. García, and J. Hyvönen, "Impact of diesel pilot distribution on the ignition process of a dual fuel medium speed marine engine," *Energy Conversion and Management,* vol. 149, pp. 192-205, 2017.

[6] J. F. Hansen and F. Wendt, "Historyand Stateofthe Art in Commercial Electric Ship Propulsion, Integrated Power Systems, and Future Trends," *Proceedings of the IEEE,* vol. 103, pp. 2229 - 2242, 2015.

[7] E. K. Dedes, D. A. Hudson, and S. R. Turnock, "Assessing the potential of hybrid energy technology to reduce exhaust emissions from global shipping," *Energy Policy,* vol. 40, pp. 204-218, 2012.

[8] A. García-Olivares, J. Solé, and O. Osychenko, "Transportation in a 100% renewable energy system," *Energy Conversion and Management,* vol. 158, pp. 266-285, 2018.

[9] J. Ling-Chin and A. P. Roskilly, "Investigating a conventional and retrofit power plant on-board a Roll-on/Roll-off cargo ship from a sustainability perspective – A life cycle assessment case study," *Energy Conversion and Management,* vol. 117, pp. 305-318, 2016.

[10] B. Zahedi, L. E. Norum, and K. B. Ludvigsen, "Optimized efficiency of all-electric ships by dc hybrid power systems," *Journal of Power Sources,* vol. 255, pp. 341-354, 2014.

[11] V. Staudt, R. Bartelt, and C. Heising, "Fault Scenarios in DC Ship Grids," *IEEE Elect r i f icat ion Magazine,* vol. 3, pp. 40 - 48, 2015.

[12] S. Castellan, R. Menis, A. Tessarolo, F. Luise, and T. Mazzuca, "A review of power electronics equipment for all-electric ship MVDC power systems," *International Journal of Electrical Power & Energy Systems,* vol. 96, pp. 306-323, 2018.

[13] Z. Jin, G. Sulligoi, R. Cuzner, L. Meng, J. C. Vasquez, and J. M. Guerrero, "Next-generation shipboard dc power system: Introduction smart grid and dc microgrid technologies into maritime electrical netowrks," *IEEE Electrification Magazine,* vol. 4, pp. 45-57, 2016.

[14] J. G. Kassakian and T. M. Jahns, "Evolving and emerging applications of power electronics in systems," *IEEE Journal of Emerging and Selected Topics in Power Electronics,* vol. 1, pp. 47-58, 2013.

[15] B. Zahedi, L. E. Norum, and K. B. Ludvigsen, "Optimization of Fuel Consumption in Shipboard Power Systems," presented at the IECON 2013 - 39th Annual Conference of the IEEE Industrial Electronics Society, 2014.

[16] B. Zahedi and L. E. Norum, "Modeling and Simulation of All-Electric Ships With Low-Voltage DC Hybrid Power Systems," *IEEE TRANSACTIONS ON POWER ELECTRONICS,* vol. 28, pp. 4525 - 4537, 2013.

[17] E. Skjong, R. Volden, E. Rodskar, M. Molinas, T. A. Johansen, and J. Cunningham, "Past, Present, and Future Challenges of the Marine Vessel's Electrical Power System," *IEEE Transactions on Transportation Electrification,* vol. 2, pp. 522-537, 2016.

[18] F. D. Kanellos, J. Prousalidis, and G. J. Tsekouras, "Optimal active power management in All Electric Ship employing DC grid technology," in *Operational Research in Business and Economics*, ed: Springer, 2017, pp. 271-284.

[19] J. Ling-Chin and A. P. Roskilly, "A comparative life cycle assessment of marine power systems," *Energy Conversion and Management,* vol. 127, pp. 477-493, 2016.

[20] F. Baldi, F. Ahlgren, F. Melino, C. Gabrielii, and K. Andersson, "Optimal load allocation of complex ship power plants," *Energy Conversion and Management,* vol. 124, pp. 344-356, 2016.

[21] E. Gagatsi, T. Estrup, and A. Halatsis, "Exploring the Potentials of Electrical Waterborne Transport in Europe: The E-ferry Concept," *Transportation Research Procedia,* vol. 14, pp. 1571-1580, 2016.

[22] L. E. Klebanoff, J. W. Pratt, C. M. Leffers, K. T. Sonerholm, T. Escher, J. Burgard*, et al.*, "Comparison of the greenhouse gas and criteria pollutant emissions from the SF-BREEZE high-speed fuel-cell ferry with a diesel ferry," *Transportation Research Part D: Transport and Environment,* vol. 54, pp. 250-268, 2017.

[23] R. H. Merien-Paul, H. Enshaei, and S. G. Jayasinghe, "In-situ data vs. bottom-up approaches in estimations of marine fuel consumptions and emissions," *Transportation Research Part D: Transport and Environment,* vol. 62, pp. 619-632, 2018.

[24] D. P. McArthur and L. Osland, "Ships in a city harbour: An economic valuation of atmospheric emissions," *Transportation Research Part D: Transport and Environment,* vol. 21, pp. 47-52, 2013.

[25] H. Winnes, L. Styhre, and E. Fridell, "Reducing GHG emissions from ships in port areas," *Research in Transportation Business & Management,* vol. 17, pp. 73-82, 2015.

[26] O. Merk, "Shipping emissions in ports," presented at the International Transport Forum, 2014.
[27] M. Tichavska and B. Tovar, "Port-city exhaust emission model: An application to cruise and ferry operations in Las Palmas Port," *Transportation Research Part A: Policy and Practice,* vol. 78, pp. 347-360, 2015.
[28] E. A. Sciberras, B. Zahawi, D. J. Atkinson, A. Juando, and A. Sarasquete, "Cold ironing and onshore generation for airborne emission reductions in ports," *Proceedings of the Institution of Mechanical Engineers, Part M: Journal of Engineering for the Maritime Environment,* vol. 230, pp. 67-82, 2014.
[29] S. G. Jayasinghe, M. Al-Falahi, H. Enshaei, N. Fernando, and A. Tashakori, "Floating Power Platforms for Mobile Cold-ironing," presented at the 2016 IEEE 2nd Annual Southern Power Electronics Conference (SPEC), Auckland, 2016.
[30] E. A. Sciberras, B. Zahawi, and D. J. Atkinson, "Reducing shipboard emissions – Assessment of the role of electrical technologies," *Transportation Research Part D: Transport and Environment,* vol. 51, pp. 227-239, 2017.
[31] G. S. Misyris, A. Marinopoulos, D. I. Doukas, T. Tengnér, and D. P. Labridis, "On battery state estimation algorithms for electric ship applications," *Electric Power Systems Research,* vol. 151, pp. 115-124, 2017.
[32] M. Zanne, M. Počuča, and P. Bajec, "Environmental and Economic Benefits of Slow Steaming," *Transactions on Maritime Science,* vol. 02, pp. 123-127, 2013.
[33] E. Skjong, E. Rødskar, M. M. Molinas Cabrera, T. A. Johansen, and J. Cunningham, "The marine vessel's electrical power system: From its birth to present day," 2015.
[34] M. D. A. Al-falahi, S. D. G. Jayasinghe, and H. Enshaei, "A review on recent size optimization methodologies for standalone solar and wind hybrid renewable energy system," *Energy Conversion and Management,* vol. 143, pp. 252-274, 2017.
[35] A. Chauhan and R. P. Saini, "A review on Integrated Renewable Energy System based power generation for stand-alone applications: Configurations, storage options, sizing methodologies and control," *Renewable and Sustainable Energy Reviews,* vol. 38, pp. 99-120, 2014.
[36] A. M. Bassam, A. B. Phillips, S. R. Turnock, and P. A. Wilson, "Design, modelling and simulation of a hybrid fuel cell propulsion system for a domestic ferry," in *PRADS2016*, Copenhagen, Denmark, 2016.
[37] C. H. Choi, S. Yu, I.-S. Han, B.-K. Kho, D.-G. Kang, H. Y. Lee*, et al.*, "Development and demonstration of PEM fuel-cell-battery hybrid system for propulsion of tourist boat," *International Journal of Hydrogen Energy,* vol. 41, pp. 3591-3599, 2016.
[38] M. Bianucci, S. Merlino, M. Ferrando, and L. Baruzzo, "The optimal hybrid/electric ferry for the Liguria Natural Parks," presented at the OCEANS 2015 - Genova, Genova, Italy, 2015.
[39] J. Han, J.-F. Charpentier, and T. Tang, "An Energy Management System of a Fuel Cell/Battery Hybrid Boat," *Energies,* vol. 7, pp. 2799-2820, 2014.
[40] A. M. Bassam, A. B. Phillips, S. R. Turnock, and P. A. Wilson, "An improved energy management strategy for a hybrid fuel cell/battery passenger vessel," *International Journal of Hydrogen Energy,* vol. 41, pp. 22453-22464, 2016.
[41] S. Trieste, S. Hmam, J. C. Olivier, S. Bourguet, and L. Loron, "Techno-economic optimization of a supercapacitor-based energy storage unit chain: Application on the first quick charge plug-in ferry," *Applied Energy,* vol. 153, pp. 3-14, 2015.
[42] Z. Jin, L. Meng, J. M. Guerrero, and R. Han, "Hierarchical Control Design for a Shipboard Power System With DC Distribution and Energy Storage Aboard Future More-Electric Ships," *IEEE Transactions on Industrial Informatics,* vol. 14, pp. 703-714, 2018.
[43] J. P. Jalkanen, L. Johansson, J. Kukkonen, A. Brink, J. Kalli, and T. Stipa, "Extension of an assessment model of ship traffic exhaust emissions for particulate matter and carbon monoxide," *Atmospheric Chemistry and Physics,* vol. 12, pp. 2641-2659, 2012.
[44] A. K. Adnanes, "Maritime electrical installations and diesel electricpropulsion," *ABB AS Marine,* 2003.

[45] B. Ghobadian, H. Rahimi, A. M. Nikbakht, G. Najafi, and T. F. Yusaf, "Diesel engine performance and exhaust emission analysis using waste cooking biodiesel fuel with an artificial neural network," *Renewable Energy,* vol. 34, pp. 976-982, 2009.

[46] Y. Du, Q. Chen, X. Quan, L. Long, and R. Y. K. Fung, "Berth allocation considering fuel consumption and vessel emissions," *Transportation Research Part E: Logistics and Transportation Review,* vol. 47, pp. 1021-1037, 2011.

[47] L. Goldsworthy and B. Goldsworthy, "Modelling of ship engine exhaust emissions in ports and extensive coastal waters based on terrestrial AIS data – An Australian case study," *Environmental Modelling & Software,* vol. 63, pp. 45-60, 2015.

[48] "Cummins engine DS72-CPGK," C. P. Generation, Ed., ed, 2012.

[49] S. Jahangiri, U. S. Kam, V. Garaniya, R. Abbassi, H. Enshaei, R. J.Brown*, et al.*, "Development of Emission Factors for Ships' Emissions at Berth," presented at the Coasts & Ports 2017 Conference – Cairns, Queensland, Australia, 2017.

[50] A. J. Baird and R. N. Pedersen, "Analysis of CO2 emissions for island ferry services," *Journal of Transport Geography,* vol. 32, pp. 77-85, 2013.

[51] S. Song, "Ship emissions inventory, social cost and eco-efficiency in Shanghai Yangshan port," *Atmospheric Environment,* vol. 82, pp. 288-297, 2014.

[52] Entec, "Defra UK Ship Emissions Inventory," https://uk-air.defra.gov.uk/assets/documents/reports/cat15/1012131459_21897_Final_Report_291110.pdf 2010.

[53] A. Stavrakaki, E. D. Jonge, C. Hugi, C. Whall, W. Minchin, A. Ritchie*, et al.*, "Service Contract on Ship Emissions: Assignment, Abatement and Market-based Instruments," Entec UK Limited August 2005 2005.

[54] C. Yin, H. Wu, F. Locment, and M. Sechilariu, "Energy management of DC microgrid based on photovoltaic combined with diesel generator and supercapacitor," *Energy Conversion and Management,* vol. 132, pp. 14-27, 2017.

[55] S. F. Tie and C. W. Tan, "A review of energy sources and energy management system in electric vehicles," *Renewable and Sustainable Energy Reviews,* vol. 20, pp. 82-102, 2013.

[56] S. Mirjalili, S. M. Mirjalili, and A. Lewis, "Grey Wolf Optimizer," *Advances in Engineering Software,* vol. 69, pp. 46-61, 2014.

[57] M. H. Sulaiman, Z. Mustaffa, M. R. Mohamed, and O. Aliman, "Using the gray wolf optimizer for solving optimal reactive power dispatch problem," *Applied Soft Computing,* vol. 32, pp. 286-292, 2015.

[58] K. S. Nimma, M. D. Al-Falahi, H. D. Nguyen, S. Jayasinghe, T. S. Mahmoud, and M. Negnevitsky, "Grey Wolf Optimization-Based Optimum Energy-Management and Battery-Sizing Method for Grid-Connected Microgrids," *Energies,* vol. 11, p. 847, 2018.

[59] S. Mirjalili, "How effective is the Grey Wolf optimizer in training multi-layer perceptrons," *Applied Intelligence,* vol. 43, pp. 150-161, 2015.

[60] M. Al-Falahi, T. Tarasiuk, S. Jayasinghe, Z. Jin, H. Enshaei, and J. Guerrero, "AC Ship Microgrids: Control and Power Management Optimization," *Energies,* vol. 11, p. 1458, 2018.

[61] PBES. (2017, August 2017). *http://www.pbes.com/wp-content/uploads/2017/06/PBES_Power-Energy_2017-06-16.pdf*.

[62] CORVUS. (August 2017). *http://corvusenergy.com/wp-content/uploads/2015/09/Corvus-Energy-Overview_Feb2016.pdf*.

[63] M. H. Rashid, "Pulse-Width-Modulation Inverters," ed: Prentice-Hall, 2004, pp. 237–248.